[44] J. H. Fuhrhop, W. Kaufmann, W. Schambil, Dtsch. Pat.-Anm. Aktenz. D 6771 (1983), Henkel.

[45] T. Kunitake, N. Nakashima, M. Shimomura, Y. Okahata, T. Kano, T. Ogawa, J. Am. Chem. Soc. 102 (1980) 6642.

[46] T. Kunitake, N. Nakashima, K. Morimitsu, Chem. Lett. 1980, 1347.

[47] T. Kunitake, N. Nakashima, S. Hayashida, K. Yonemori, Chem. Lett. 1979, 1413.

[48] N. Nakashima, H. Fukushima, T. Kunitake, Chem. Lett. 1982, 1555.

[49] J.-H. Fuhrhop, H. H. David, unpublished.

[50] H. Bader, H. Ringsdorf, J. Skura, Angew. Chem. 93 (1981) 109; Angew. Chem. Int. Ed. Engl. 20 (1981) 91.

[51] M. Shimomura, T. Kunitake, J. Am. Chem. Soc. 104 (1982) 1757.

[52] T. Kunitake, Y. Okahata, S. Yasunami, J. Am. Chem. Soc. 104 (1982) 5547.

[53] H. Ihara, Y. Hashiguchi, T. Kunitake, Chem. Lett. 1983, 733.

[54] E. M. Arnett, J. Chao, B. J. Künzig, M. V. Stuart, O. Thompson, R. J. Verbiar, J. Am. Chem. Soc. 104 (1982) 389.

[55] T. Kunitake, T. Sakamoto, J. Am. Chem. Soc. 100 (1978) 4615.

[56] R. A. Moss, G. Bizzigotti, J. Am. Chem. Soc. 103 (1981) 6512.

[57] Y. Murakami, A. Nakano, A. Yoshimatsu, K. Fukuya, J. Am. Chem. Soc. 103 (1981) 728.

[58] K. Ohkubo, K. Sugahara, K. Yoshinaga, R. Ueoka, J. Chem. Soc. Chem. Commun. 1980, 637.

[59] M. F. Czarniecki, R. Breslow, J. Am. Chem. Soc. 101 (1979) 3675.

[60] J. N. Israelachvili, S. Marcelja, R. G. Horn, Q. Rev. Biophys. 13 (1980) 121.

[61] T. Kunitake, Y. Okahata, M. Shimomura, S. Yasunami, K. Takarabe, J. Am. Chem. Soc. 103 (1981) 5401.

[62] T. M. S. Chang: Artificial Cells, Thomas, Springfield, Ill. 1972; Introduction to Artificial Kidney, Artificial Liver, Artificial Cells, Plenum Press, New York 1978.

[63] T. M. S. Chang, J. Macromol. Sci. Chem. A 10 (1976) 245.

[64] Bilayer membranes from water-soluble polyvinyl alcohol and dimethyl-(dioctadecyl)ammonium bromide (1:1) have also been described: S. Hayashida, H. Sato and S. Sugawara, Chem. Lett. 1983, 625.

[65] S. W. Fox, Naturwissenschaften 56 (1969) 1.

[66] A. L. Lehninger: Biochemistry, Worth, New York 1970, p. 783 ff.

[67] J.-H. Fuhrhop, J. Mathieu, unpublished.

[68] M. Calvin, Acc. Chem. Res. 11 (1978) 369.

[69] M. S. Tunuli, J. H. Fendler, J. Am. Chem. Soc. 103 (1981) 2507.

[70] G. Gregoriadis, A. C. Allison: Liposomes in Biological Systems, Wiley, New York 1980.

Photochemical Hole Burning: A Spectroscopic Study of Relaxation Processes in Polymers and Glasses

By Josef Friedrich and Dietrich Haarer*

Photochemical hole burning is a special type of saturation spectroscopy in the optical domain having many analogies with NMR methods. The holes, which are burnt with laser irradiation, appear as small indentations in the absorption spectra of dye molecules which are doped into a polymer or glass in minute concentrations. Based on their narrow line width, photochemical holes can be regarded as highly sensitive spectroscopic probes. They can be used to detect small perturbations of the system by external parameters, giving rise to line-shifts and broadenings. Besides the many well documented, spectroscopic applications of hole burning, it may offer interesting future developments for the spectroscopy of biomolecules and for high-density data storage.

1. Introduction

The optical properties of many crystalline and polymeric organic solids are frequently dominated by guest molecules. Guest molecules can either be impurities or doping materials. It has, for example, been known from the early days of low temperature spectroscopy of crystalline organic materials that impurities in low concentrations (10^{-4} mol/mol) can dominate the emission spectra of crystalline host matrices[1,2].

This article deals with hole burning spectroscopy of organic host-guest systems. This spectroscopic method was discovered in 1974 by two Soviet research groups[3-5]. Photochemical hole burning (PHB) spectroscopy is a special kind of saturation spectroscopy: With narrow-band excitation very narrow and stable photochemical holes can be "burned" into the absorption bands of guest molecules. From the line width and line shape of these holes one can

obtain information about both the host and guest systems (examples of photochemical holes are shown in Figs. 14, 19, 30, and 31). Most attractive is the very high optical resolution of the hole burning method. In this article we shall mainly focus on the spectroscopy of glasses and polymers, since the high resolution aspects of the new method are especially useful in this field.

In this context we mention that organic host-guest systems are also interesting from the viewpoint of applications. Examples are sunlight-collectors which use organic molecules in polymer or glass matrices to scatter diffuse sunlight into a small solid angle[6,7]. Other, more complex host-guest systems, which are still not completely understood, are polymeric photoconductors[8,9], photographic layers[10], and biological light-harvesting pigments[11].

2. Energy Bands, Localized Excitations, and Phonons

The optical properties of organic solids which are doped with dye molecules are determined both by the absorption

[*] Prof. Dr. D. Haarer, Prof. J. Friedrich
Physikalisches Institut der Universität
Postfach 3008, D-8580 Bayreuth (FRG)

spectrum of the guest and that of the host. The host states are characterized by bands of bandwith B (Fig. 1). The origin of the band states is the close packing of the host molecules leading to a strong molecular interaction. Band states have dispersive character, i.e. the excitation energy is, in most cases, delocalized over many molecules[12, 13] (excitonic state). In contrast to the band states, the excited states of the guest molecules are localized. The localized states are referred to as matrix-isolated because they are more or less decoupled from the host states. Many systems which absorb in the visible region are matrix-isolated. The host system is frequently chosen such that its intrinsic absorption is in the UV region of the spectrum. In the following we will focus our attention on matrix-isolated systems and thus do not have to deal with the band-states shown in Figure 1. We will, instead, focus on the states S_1, S_2 which arise from doping and which are termed extrinsic and will investigate their electronic, vibronic (v), and phonon satellites. Examples of such systems are amorphous polystyrene (matrix) doped with phthalocyanine (guest) or crystalline durene (1,2,4,5-tetramethylbenzene) (matrix) doped with naphthacene (guest). The concentrations of the dopant are usually very low (10^{-4} to 10^{-6} mol/mol).
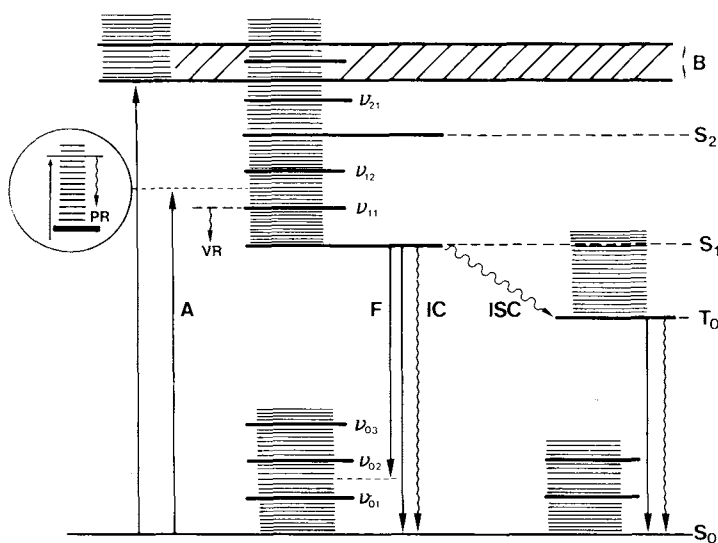

Phthalocyanine   Naphthacene

Fig. 1. Energy level scheme of a dye molecule in an organic glass or polymer matrix. B: Electronic band states of the host system (exciton band); S_i, T_i: Singlet and triplet levels of the guest molecule; v_{ij}: Vibrational levels of the guest molecule in its electronic state i. The levels which appear as a quasi-continuum correspond to phonon states of the host. PR: phonon relaxation; VR: vibrational relaxation; IC: internal conversion; ISC: intersystem crossing; A: absorption; F: fluorescence.

The probability per unit time of an optical transition from the ground state S_0 to an electronic state of the guest molecule (for instance S_1) can be calculated via Fermi's golden rule:

$$P_{10} = \frac{2\pi}{\hbar} |\langle \Psi_1|\hat{H}_{rad}|\Psi_0\rangle|^2 g(E-E_1) \tag{1}$$

where Ψ_0 is the electronic wave function of the ground state S_0, Ψ_1 is the wave function of the first excited state, and $g(E-E_1)$ is the normalized absorption line shape
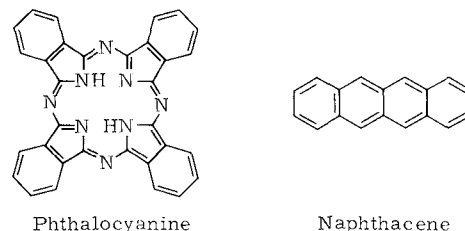
function. $\hat{H}_{rad}$ characterizes the interaction of the molecule with the radiation field of the light source:

$$\hat{H}_{rad} = -\vec{\mu}\cdot\vec{E}(t) \tag{2}$$

Equations 1 and 2 show that the transition probability P_{10} is proportional to the square of the transition dipole moment $\vec{\mu}_{10} = \langle \Psi_1|\vec{\mu}|\Psi_0\rangle$, where $\vec{\mu}_{10}$ is related to the oscillator strength f_{10} of the transition under consideration (see e.g. [14]):

$$|\mu_{10}|^2 = f_{10}\,[3\hbar\,e^2/(4\pi m\,c\,\bar{v}_{10})] \tag{3}$$

where $\bar{v}_{10}$ is the optical transition energy in cm^{-1}.

The oscillator strength f_{n0} can be obtained directly from measurements of the extinction coefficient ε_{n0}. The index n labels the transition n←0 whose absorption spectrum is being considered. One can write

$$f_{n0} = \ln 10 \cdot \frac{4\varepsilon_0 m c^2}{e^2 N_A \cdot n_0} \int_{-\infty}^{\infty} \varepsilon_{n0}\,d\bar{v}_{n0} \tag{4}$$

where N_A is Avogadro's number, n_0 is the refractive index of the material, and ε_0 is the dielectric constant.

So far, only electronic excitations have been considered (with the additional assumption of dealing with allowed transitions). Besides the electronic excitations, molecular spectra also reflect vibrational degrees of freedom. The relative intensity of the electron-vibration bands is given by the Franck-Condon principle, which determines the coupling of the intramolecular vibrations of the guest molecules, which have well-defined energies up to several thousand wave numbers; the same principle also determines the coupling of lattice modes (phonons) to the electronic transition. Typical phonon energies lie in the range 10 to 100 cm^{-1}; they have a continuum character (Fig. 1). In the following we consider the coupling of a "normal lattice mode" q_i of frequency Ω_i. Figure 2 shows two electronic energy levels E_0 and E_1. On each of these levels one can build up excitations of harmonic oscillators with energies $\hbar\Omega_i$. As can be seen from the figure, an electronic excitation from E_0 to E_1 leads to a change in equilibrium distance from $q_i = 0$ in the ground state to $q_i = q_{i0}$ in the excited state. The corresponding energy change is proportional to the force constant $K_i = m_i\Omega_i^2$ of the harmonic oscillator with frequency Ω_i and mass m_i:

$$E_{pi} = \tfrac{1}{2}K_i q_{i0}^2 = \tfrac{1}{2}m_i\Omega_i^2 q_{i0}^2 \tag{5}$$

The energy E_{pi} corresponds to half the Stokes-shift between the maxima of the absorption and emission spectra.

If one wants to calculate optical spectra, the transition probabilities to the vibrational levels $\Phi_{ni}(v)$ have to be cal-
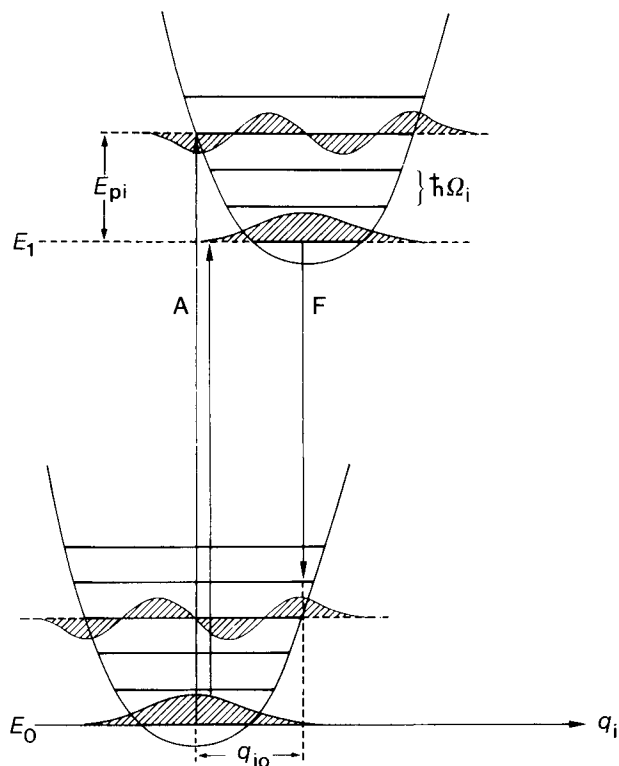
Fig. 2. Energy diagram for interpreting the phonon sideband spectra in terms of configurational coordinates: q_i represents a normal mode of the lattice. The arrows correspond to zero-phonon and three-phonon transitions in absorption and emission, respectively (see text).

culated. Here, the index n stands for the electronic excitation, index i labels the i-th lattice mode of frequency $\hbar\Omega_i$, and v labels the number of excited vibrational quanta in the mode i.

To simplify the calculation, several approximations have to be introduced. The first, is the *harmonic approximation*, which assumes that all lattice modes are independent of another and are described by parabolic potentials; the second, is the *low temperature approximation*, which assumes that in the lowest electronic state only the zero point vibration is excited; the third approximation is the assumption of *linear electron-phonon coupling*, which assumes identical force constants in the ground state E_0 and excited state E_1.

In most experiments the above assumptions are well fulfilled. (Some details have to be modified for calculation of the optical line widths.)

The transition probability $\Psi_1 \leftarrow \Psi_0$ can be calculated using the Franck-Condon principle, which states that the electronic excitation is so rapid that the lattice coordinates q_i cannot follow. Hence, in Figure 2 the optical transitions can be symbolized by vertical arrows. With the above assumptions the transition probability can be calculated from the lowest vibrational state (00) to the vth level of the lattice mode q_i in the excited electronic state

$$P_{1i,00}(v) = \frac{2\pi}{\hbar} |\langle \Psi_1 \Phi_{1i}(v)|\hat{H}_{rad}|\Psi_0 \Phi_{0i}(0)\rangle|^2 g(E - E_1 - v\hbar\Omega_i)$$

(6)

$$= \frac{2\pi}{\hbar} |\langle \Phi_{1i}(v)|\Phi_{0i}(0)\rangle|^2 |\langle \Psi_1|\hat{H}_{rad}|\Psi_0\rangle|^2 g(E - E_1 - v\hbar\Omega_i)$$

The line shape function of equation (6) leads to narrow peaks with spacing $\hbar\Omega_i$, characterizing the absorption spectrum of the electronic transition $1 \leftarrow 0$. The intensity of the narrow peaks is given by the overlap of the harmonic oscillator wave functions of Figure 2. Figure 3a shows the transition probability for two modes i and j calculated with the aid of equation (6). For the sake of clarity, we have drawn the absorption and emission spectra separately. In order to obtain the complete spectrum, all modes i have to be summed. Figure 3b shows a spectrum which results from superposition of modes i and j. The *zero-phonon line* ($v = 0$) dominates the whole spectrum. There are two reasons for this: First, the zero-phonon lines of all lattice modes i,j... add at the electronic origin $E_1 - E_0$. Second, the width of the zero-phonon line is narrower because its relaxation is prohibited to some extent by the large energy splitting $E_1 - E_0$. The adjacent lattice states spaced by $n\hbar\Omega_i$ and $n\hbar\Omega_j$ relax on a much faster time scale. The envelope of all phonon excitations is termed a *phonon sideband*.
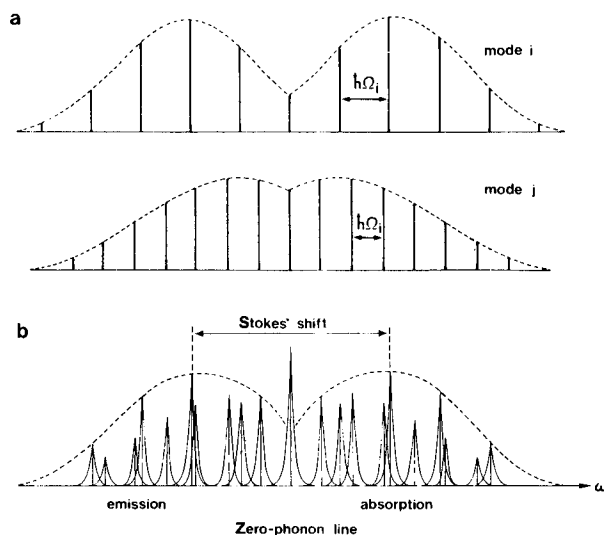

Fig. 3. a) Transition probabilities for two lattice modes i and j [see eq. (6)]; b) superposition of the two modes i and j. The intensities of both modes add up at the zero-phonon frequency (line coincidence); however, they do not add up in the multi-phonon transitions.

We are interested in calculating the line shapes quantitatively. Figure 4 therefore shows a typical line profile of an electronic transition including its phonon sideband (see Section 3). An important quantity is the Lorentzian zero-phonon line $z(\omega)$ with its integrated area α and its line width γ. A second characteristic feature is the phonon sideband $p(\omega)$ with its integrated area $(1 - \alpha)$. The line shape of the phonon sideband is given by the overlap integrals of equation (6); these correspond to a Poisson distribution (see e.g. [15]). In many cases an approximation using a Gaussian profile is completely adequate[15, 16, 17]. The total line shape of the $1 \leftarrow 0$ transition is a normalized superposition of $z(\omega)$ and $p(\omega)$. The transition is characterized by the Debye-Waller factor α, which gives the relative intensity I_0 of the zero-phonon line normalized by comparison with the total intensity I_g. Figure 5 shows an experimentally determined guest-host phosphorescence spectrum[18]: In Fig-

Angew. Chem. Int. Ed. Engl. 23 (1984) 113–140

115

$\alpha z(\omega - \omega')$

v

Δ

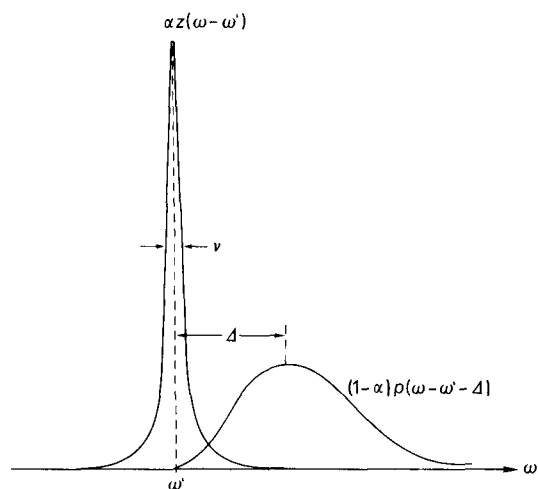$(1 - \alpha) p(\omega - \omega' - \Delta)$

ω

ω'

Fig. 4. General line shape function of an electronic excitation of a guest molecule in a solid host matrix: Schematic view of a zero-phonon line and phonon sideband.

ure 5b the zero-phonon line is the dominating feature and in Figure 5a the phonon sideband dominates. The first case is referred to as *weak* electron-phonon coupling and the second, as *strong* electron-phonon coupling. For high-resolution hole burning spectroscopy one needs systems with strong zero-phonon lines to yield the required optical resolution.

a

b

4800   4600
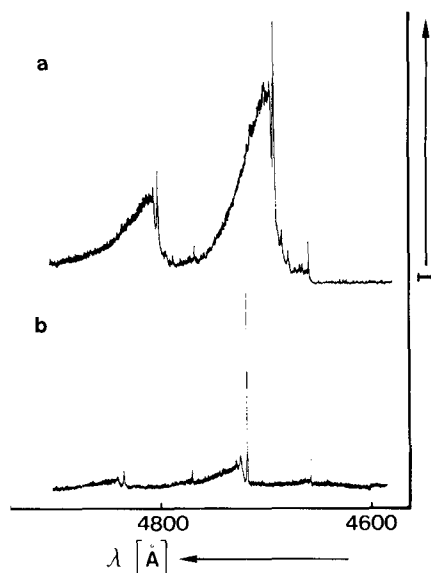
$\lambda \; [\text{Å}]$

Fig. 5. Phosphorescence spectra of two trap states in the charge-transfer single crystal naphthalene-tetrachlorophthalic anhydride. a) Purified material: The trap state is strongly coupled to the lattice, i.e. the relative intensity of the phonon sideband is large. b) Unpurified material: The trap state is weakly coupled to the lattice; the relative intensity of the phonon sideband is small. A trap-state is a localized excited state of a crystal and can, for example, be produced by doping or by the presence of impurities in natural abundance.

The Debye-Waller factor α is extremely relevant for hole burning experiments. It follows explicitly from equation (6) if one compares the contribution of all modes to the zero-phonon line, namely $\sum_i |\langle \Phi_{1i}(0) | \Phi_{0i}(0) \rangle|^2$, with the total intensity. Since the total intensity is normalized, one obtains

$$\alpha = I_0 / I_g = \sum_i |\langle \Phi_{1i}(0) | \Phi_{0i}(0) \rangle|^2 \qquad (7)$$

As $T \to 0$, α can readily be calculated (see e.g. [19]), giving

$$\alpha(T=0) = \exp \left(-\frac{1}{2} \sum_i \frac{m_i \Omega_i}{\hbar} q_{i0}^2 \right) \equiv \exp(-S) \qquad (8)$$

If only a single phonon mode is considered, S has a simple physical interpretation: It corresponds to the number of vibrational quanta which are excited in the maximum of the phonon sideband. If the case shown in Figure 2 is taken, one gets an S-value of 3. The "Franck-Condon gap" Δ_i (half the Stokes-shift) can also be calculated from the one-mode model shown in Figures 2 and 4:

$$\Delta_i = S_i \hbar \Omega_i \qquad (9)$$

For S-values > 5, one is dealing with strong electron-phonon coupling. In such cases one cannot expect to observe a narrow zero-phonon line [eq. (8)]. Especially in the case of rather strong electron-phonon coupling, the "one-mode" model is quite often good, because usually a single mode couples more strongly than the others and, thus, dominates the optical spectrum.

3. Optical Line Shapes in Perfect Lattices

The optical properties of guest molecules are strongly influenced by the nature of the host lattice. For this reason one can consider a guest molecule as a sensitive probe for the structure and dynamic properties of the host lattice. To exemplify the host-guest interaction we consider a matrix-isolated molecule. Its excited state lifetime T_{10} is given by various relaxation processes, such as fluorescence (F), intersystem crossing (ISC), internal conversion (IC), and vibrational relaxation (VR) (see e.g. [20] and Fig. 1). From Heisenberg's uncertainty relation the *natural line width* γ_0 is

$$\gamma_0 = 1/T_{10} \qquad (10)$$

γ_0 is given as the full width at half-height (FWHH) and is expressed in units of $2\pi/s$. For singlet states S_1, lifetimes of 10^{-8} to 10^{-9} s are typically encountered; therefore, the γ_0 values lie in the range 100 MHz to 1 GHz. If one wants to measure natural line widths, typically an optical resolution $\omega_0/\gamma_0 = 10^7 - 10^8$ is required (ω_0 is the frequency of the optical transition).

So far we have neglected the influence of the lattice, which reduces the lifetime T_{10} to T_1 by introducing new radiationless decay channels[21]. In addition to the relaxation phenomena, the host-guest interaction introduces mechanical strain; it also leads to electrostatic and to van der Waals' interactions, shifting the molecular level by a "solvent shift" D[22]. In the case of a perfect host lattice, all molecules experience identical shifts and, hence, their optical transitions coincide (Fig. 6). The width of this ideal line at $T=0$ is given by its lifetime T_1. Upon increasing the temperature, the thermal motion of the lattice increases and leads to an additional line-broadening mechanism, termed *phase relaxation* (see e.g. [23,24]). We would like to describe
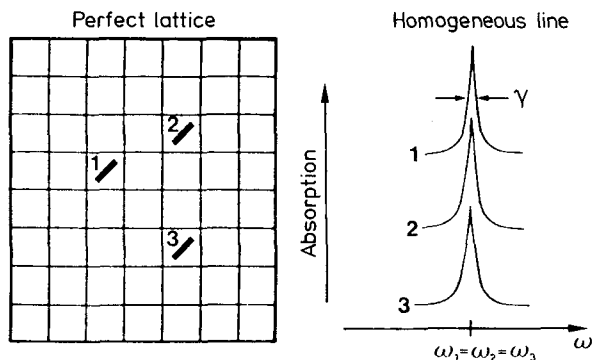
116

Fig. 6. Schematic view of the optical absorption lines of three (identical) guest molecules in a perfect crystal. The three lines have identical transition frequencies.

this relaxation process on a qualitative level. If a whole ensemble of molecules is excited with a coherent light source, an ensemble of molecules oscillating in phase with each other and with the external light source results. In this way, a macroscopic polarization $\vec{P}$ is induced which can be expressed as a vectorial sum of all molecular transition dipole moments

$$\vec{P} = \vec{P}_0 e^{i[(E_1 - E_0)/\hbar]t} \ ; \qquad \vec{P} = \langle \vec{\mu}_{10}(t) \rangle \qquad (11)$$

Equation (11) describes a complex vector rotating with the laser frequency

$$\omega_L = (E_1 - E_0)/\hbar$$

(In a coordinate system which rotates with frequency $\omega_{01} = (E_1 - E_0)/\hbar$, the fast-phase factor of eq. (11) is 1; see Section 6.)

If an individual molecule of the large ensemble is considered, a thermal motion in its neighborhood will change its energies from E_0 to $E_0 + \Delta E_0$ and from E_1 to $E_1 + \Delta E_1$. As a consequence, the characteristic frequency of the transition moment is shifted by the amount $\varepsilon = (\Delta E_0 - \Delta E_1)/\hbar$. This "detuning" leads to a phase loss of the molecule. Since the thermal motions of the lattice have a stochastic nature, ε is also stochastic and thus leads, within the time interval T_2^* (phase relaxation time), to a statistical distribution. During this time the various transition moments become out-of-phase and, thus, the macroscopic polarization drops to $\vec{P}_0/e$.

These considerations are only valid if the lattice fluctuations can be regarded as being stochastic, i.e. if a motion at time $t + t'$ is completely independent of one at time t. This is valid for $t' \gg \tau_c$, where τ_c is the correlation time describing lattice fluctuations. If one applies Heisenberg's uncertainty principle to the decay of the macroscopic polarization,

$$\gamma_h = 1/T_2 \geqslant 1/T_1 \qquad (12)$$

results, where γ_h is the homogeneous line width: this reflects the dynamic influence of the lattice on the probe molecule. As mentioned previously, $T_2 \to T_1$ as $T \to 0$ K, which is a consequence of the third law of thermodynamics. At $T = 0$ K the stochastic motions of the lattice are "frozen

out". The lattice has a "sharp" energy level and thus its entropy is zero.

The lattice fluctuations are caused by phonons, which at thermodynamic equilibrium are created and destroyed with the boundary condition of a mean occupation number $\langle n \rangle$ given by

$$\langle n \rangle = 1/(e^{\frac{\hbar\omega}{kT}} + 1) \qquad (13)$$

One can, therefore, argue that the fluctuations of an excited state are caused by quasi-elastic scattering via phonons[25,26,27]. This is shown schematically in Figure 7: A phonon is absorbed in the ground state Ψ_0 of the scattering center. This changes the energy of the state Ψ_0 by a small amount ΔE_0. If the coupled system of molecule plus phonon absorbs a light quantum, it does so at an energy $(E_1^* - E_0^*)$, which is slightly different from that of a "phonon-less" transition at $(E_1 - E_0)$. This is due to a slightly different charge distribution in the probe molecule in the excited state. Since the phonon is re-emitted to the lattice, one refers to the above process as elastic scattering. These scattering processes lead to an increase in line width of the order $(\langle (\Delta E_0 - \Delta E_1)^2 \rangle)^{1/2}$. Clearly, as $T \to 0$ K such scattering processes disappear [eq. (13)], since at $T = 0$ no thermal phonons are available.
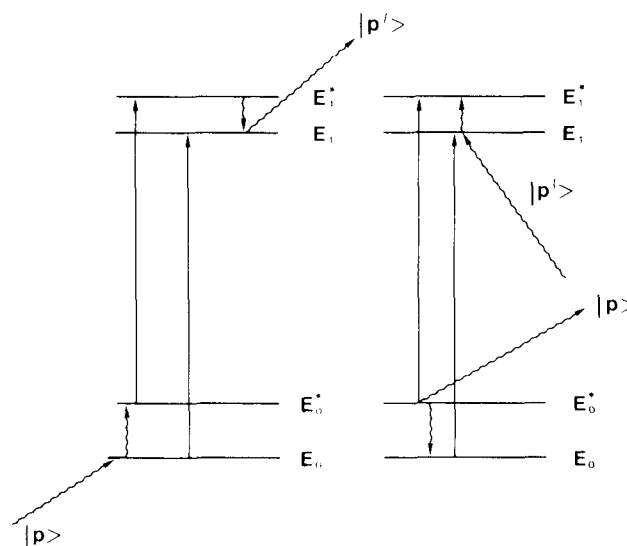
Fig. 7. Energy diagram for elastic phonon scattering involving two different electronic levels (0,1). The electronic transitions are drawn with straight arrows, the phonon transitions with wiggly arrows.

In this case, γ_h is, according to eq. (12), exactly determined by the inverse of the lifetime T_1. The discussion presented here shows that the homogeneous line width as a function of temperature is a characteristic probe for dynamic processes in the lattice.

At this point we want to make some remarks concerning the line widths. We have shown earlier in this section that the phase relaxation is given by the decay of the macroscopic polarization. In mathematical terms, this time dependence is described by the autocorrelation function of the dipole moment[28]:

$$C(t) = \langle \vec{\mu}(0) \vec{\mu}(t) \rangle \qquad (14)$$

The autocorrelation function can be viewed as a mathematical scheme which correlates a physical parameter (here the macroscopic dipole moment) at time t with the same quantity at $t = 0$. The average brackets in equation (14) reflect that C is a macroscopic quantity. The optical line shape is given by the Fourier transform of the autocorrelation function of the dipole moment:

$$L(E) = \frac{1}{2\pi} \int_{-\infty}^{+\infty} C(t) e^{-iEt/\hbar} \, dt \qquad (15)$$

The decay of C is given by T_2^* and T_1 for times $t \gg \tau_c$[29]. For exponential decay of C, $L(E)$ is given by a Lorentzian line shape. If only two states are considered (i.e. Ψ_0, Ψ_1), equation (15) yields directly

$$L(E) = |\vec{\mu}_{01}|^2 g(E - E_1) \qquad (16)$$

where g is the normalized line shape function introduced in equation (1).

4. Optical Spectra in Glass Matrices

The optical spectra of guest molecules in glassy matrices are very different from those in crystalline matrices. To understand this phenomenon, one has to grasp the basic difference between a crystal and a glass: The glass transition is not a real phase transition, even though many thermodynamic properties exhibit discontinuities there[30-32]. The glass transition has certain kinetic aspects which we will discuss briefly. If the temperature of a host-guest system is lowered through the range in which the glass transition occurs, the intrinsic viscosity of the liquid increases by many orders of magnitude. The liquid finally freezes at a fictitious temperature T_x. To define this temperature, we have to perform a *gedankenexperiment:* We freeze the liquid slowly, maintaining thermodynamic equilibrium. The increasing viscosity of the solution leads to increasing relaxation times and, hence, equilibrium can only be maintained down to a temperature T_x. At this point we quench the liquid to temperatures below which the liquid freezes, i.e. is in a glassy state. We can then assume that the potential distribution of the glass corresponds to that of the liquid at temperature T_x. Clearly, T_x depends on the cooling rate. The thermodynamic properties of a glass therefore depend on the sample's cooling history. Hence, a glass is a *non-equilibrium state*[33]. Each cooling cycle leads to a different point in the configurational space. Figure 8 shows a cross section through the configurational space along a coordinate q. The figure shows that a glass has entropy even at absolute zero[33], since it can occupy various configurations. This is in contrast to the typical situation for a crystal, whose configuration is well defined at $T = 0$. In a glass one can think of relaxation processes (e.g. between the states 1 and 2 of Fig. 8) leading to an energy uncertainty, which will eventually be reflected in the optical spectra of glassy materials.

Figure 8 suggests an approach to a quantum mechanical interpretation of the glassy state[34,35]. The random potential given in Figure 8 can be represented as a distribution
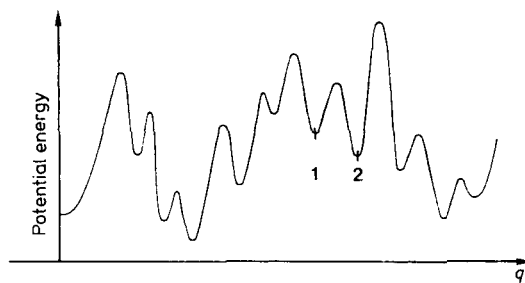

Fig. 8. Cross section through the configurational space of a glass along a fictitious coordinate q (see text).

of double-well potentials. The dynamics of the glassy state can be modeled by the dynamics of double-well potentials whose parameters are determined by an appropriate distribution function. The physics of the systems is determined by this distribution function[36,37]. Measurements of specific heat (C_p) below 1 K allow conclusions to be drawn about the glass distribution function, but only over narrow energy ranges[37,38] (see Section 13).

For double-well potentials the nomenclature of "two-level systems" (TLS) has been used to describe the two lowest eigenstates of the system. The TLS states seem to have a high spectral density at very low energies and this is responsible for the so-called thermal anomalies: At temperatures below 1 K the specific heat increases linearly with temperature (crystal $\sim T^3$) and is time-dependent[39,40] and the thermal conductivity increases with T^2 (crystal $\sim T^3$); both the velocities of sound and that of light in glassy systems are temperature-dependent[41]. In the past few years it has become clear that TLS also influence the optical properties of amorphous materials[42-46].
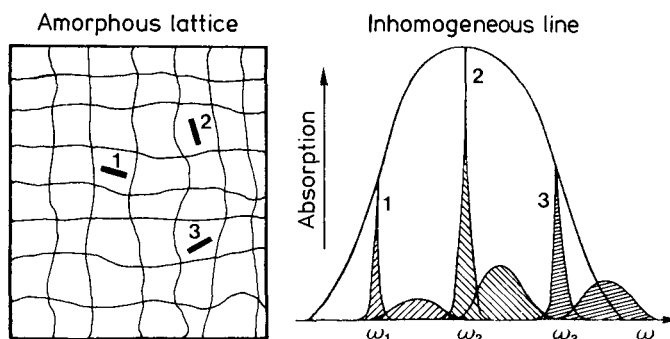

Fig. 9. Schematic view of the optical absorption of three (identical) guest molecules in an amorphous host. In contrast to the situation in a crystalline lattice, the lines appear at different transition frequencies. The broad sidebands represent the phonon spectra of molecules 1, 2 and 3, respectively.

As pointed out previously, the microscopic environment of a "solvent" molecule in a glass is random (Fig. 9). Therefore, the "solvent shift" D is, in contrast to the situation encountered in crystalline systems, not uniform but given by a statistical distribution (site distribution). The latter is usually assumed to be Gaussian:

$$G(D) = 2\sqrt{\frac{\ln 2}{\pi}} \cdot \frac{1}{\Gamma} \exp\left\{ -\frac{4(D - D_0)^2 \ln 2}{\Gamma^2} \right\} \qquad (17)$$

In organic glasses this distribution can span several hundred wave numbers. Similar distributions are observed for crystals with imperfections; however, in the latter case the line width is only of the order of several wave numbers. The width of the site distribution Γ (full width at half-hight, FWHH) is termed the *inhomogeneous* line width. Figure 9 gives a schematic view of the spatial fluctuations of the site geometry and the corresponding optical absorption profiles. (Besides the spatial fluctuations, there are also fluctuations in the time domain which are responsible for the *homogeneous* line width.) One goal of this article is to discuss methods for measuring individual line shape functions (1, 2, and 3 in Fig. 9) despite the inhomogeneous line broadening phenomena which characterize the glassy state and which, under normal conditions, mask the line shape. A second goal is to relate the line shape profiles to the specific degrees of freedom of the amorphous host matrix (TLS).

5. The Optical Two-Level System Interacting with a Coherent External Field

In the following we briefly compare spectroscopic experiments in the frequency domain (especially optical hole burning) with those in the time domain. Both types of experiments can, under certain conditions, give the same information.

The mathematical framework necessary to describe optical relaxation processes is almost identical with that used in the theory of spin resonance phenomena. This was proved by *Feyman et al.*[47] who described the general equivalence between an optical two-level system and a spin-1/2 system. For the optical two-level system we define the initial and final states as the electronic ground state and the lowest allowed excited state (S_1), respectively. Bearing the basic properties of a spin 1/2 system in mind, we point out some qualitative differences between the optical two-level system and a spin-1/2 system.

a) For optical two-level systems the relation $E_1 - E_0 \gg kT$ holds in general. The longitudinal relaxation time T_1 therefore exists only for the excited state E_1 with a measurable rate. It corresponds to the optical lifetime. The lifetime of the ground state can be assumed to be infinite (i.e. no measurable thermal population of E_1). In other words, the two-level system tends towards a state of complete "polarization" if no radiation is absorbed. A state of complete polarization can, in the case of spin resonance, only be achieved at infinitely high magnetic fields (or infinitely low temperatures). In this highly polarized state all spins are aligned. A completely different picture applies to energy-conserving dephasing processes, which can occur in both the ground *and* excited states. Dephasing processes are usually due to phonon scattering. For optical systems the condition $T_2 = T_1$ is only fulfilled in exceptional cases (i.e. at very low temperatures).

b) In optical systems spontaneous emission processes play an important role. This behavior is quite different from

magnetic systems; the ω_{01}^3-dependence of the spontaneous emission clearly favors optical frequencies. The optical spectroscopic methods of fluorescence and phosphorescence are therefore mostly based on spontaneous emission processes. Similar experiments would be difficult, if not impossible, with ESR and NMR spectroscopy. Spin resonance experiments are, thus, based on coherent phenomena as described by the Bloch equations. Only after the advent of lasers as coherent light sources was it possible to perform coherent Bloch-type experiments in the optical region[48].

c) In optical spectroscopy the sample dimensions are, in general, large compared to the wavelength. In addition to the Bloch equations, Maxwell's equations therefore must also be applied. Both sets of equations are often referred to as the Bloch-Maxwell equations.

d) In magnetic resonance phenomena the Larmor frequency of the precessing spin ensemble has a geometric interpretation: The magnetization vector precesses, as long as it has a component perpendicular to the field direction, at the Larmor frequency. It can therefore be detected with appropriate detector coils which pick up an x−y magnetization. The "optical Larmor frequency" $\omega_{10} = (E_1 - E_0)/\hbar$ has no real geometric relevance, i.e. there is no precession in real x, y, z space.

In connection with the above considerations we wish to summarize the basic relations which link optical line width data with the corresponding optical relaxation times. The equations which will be given below can be derived by solving the time evolution of the density matrix of a two-level system driven by a coherent electric field, and represent the optical analogues of Bloch's equations for a precessing spin. They basically describe the phase decay of an ensemble of optically excited molecules (for a review see [49, 50]).

If the pure dephasing time of the molecules is defined as T_2^* and the lifetime in the excited state as T_1, one arrives at an effective decay time of the total ensemble of excited molecules

$$1/T_2 = 1/T_1 + 2/T_2^* \tag{18}$$

In contrast to similar expressions derived in spin resonance spectroscopy, equation (18) is not symmetrical in T_1 and T_2^*. The reason for this difference is that for an optical two-level system the excited state cannot be populated thermally. This has as the consequence that only one of the two states (the excited one) can decay with T_1. Scattering processes with characteristic time T_2^* can, however, occur in both the ground and excited states.

Knowing T_1 and T_2, one can calculate the optical line width (FWHH; in units of $2\pi/s$) of an optical two level system as

$$\gamma_h = \frac{1}{T_2} \sqrt{1 + \omega_1^2 T_1 T_2} \tag{19}$$

where ω_1 is the Rabi frequency, proportional to the amplitude of the electric field vector of the light wave. The characteristic time for driving the molecular ensemble from the

Angew. Chem. Int. Ed. Engl. 23 (1984) 113–140

119

ground state to a state with equal population of the ground and excited states is $t = \pi/2\omega_1$; ω_1 is defined as

$$\omega_1 = \bar{\mu}_{10}\bar{E}_0/\hbar \qquad (20)$$

where $\bar{\mu}_{10}$ is the dipolar matrix element of the optical transition. Equation (19) shows that the optical line width increases at high light-intensities. This line-broadening is referred to as power broadening. In hole burning spectroscopy, one usually tries to avoid power broadening by performing the experiments at low power levels where the following condition holds

$$\omega_1^2 \ll \frac{1}{T_1 \cdot T_2} \qquad (21)$$

These lower power levels require longer irradiation times for PHB photochemistry. It should be mentioned that the phenomenon of power broadening is completely different from the so-called "photochemical saturation broadening" (Section 9), which arises from bleaching of the photoactive molecules over a narrow frequency range.

As mentioned previously, excessively high light-intensities in hole burning experiments are avoided since power broadening would otherwise result. However, the methods used in transient spectroscopy, which are summarized in the following section, require high light-intensities. For these experiments equation (21) cannot be fulfilled, and the light field chosen has to be high enough to perform the transient changes in times small compared to T_1 and T_2^* (adiabatic rapid passage, see [51]).

6. Transient Experimental Methods for Determining Optical Relaxation Times

6.1. Free Induction Decay

A very useful method for measuring the optical relaxation time T_2 in the *time domain* is optical free induction decay (FID or OFID). In the FID experiment, a macroscopic polarization is generated in the sample by irradiating it with coherent light. The polarization field of the sample is then superimposed on the incident light field, leading to a beat frequency between the two oscillations. To observe FID experimentally, one has to "switch" the laser frequency fast (compared to T_1, T_2^*) into and out of the molecular resonance frequency. This can be achieved either by Stark-switching the molecular energy levels[52-54] or by rapidly switching the laser frequency[55].

The optimal experimental condition for observing FID arises if the polarization corresponds to equal population of the ground and excited states. This is achieved by irradiating a resonant field during the time interval $t_{\pi/2}$, thereby rotating the polarization by $\pi/2$. To achieve a $\pi/2$-rotation, the condition

$$\omega_1 \cdot t_{\pi/2} = \pi/2 \qquad (22)$$

has to be fulfilled.

After generating the above polarization, the laser frequency is quickly shifted from ω_{01} to $\omega_{01} + \delta\omega$. It is impor-

tant that $\delta\omega$ be several times larger than the homogeneous line width. In this case the beat phenomenon between the (complex) polarization $\bar{P}$ and the external field decays according to the following relation:

$$\bar{P}(t) = \bar{\mu}_{01} N \exp\{i\delta\omega t\} \cdot \exp\{-t/T_2\} \qquad (23)$$

Equations (23) and (24) show no high frequency oscillations with ω_{01}, since they are formulated in a reference frame rotating at frequency ω_{01} (rotating frame description).
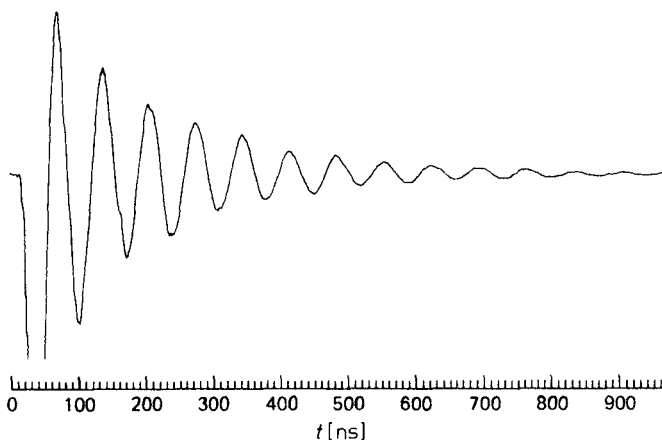

Fig. 10. Optical free induction decay (OFID) of the praseodymium(III) ion in lanthanum trifluoride [56].

In equation (23), N is the number of molecules in the ensemble and $\delta\omega$ is the beat frequency between the sample polarization and the light wave. Figure 10 shows an FID signal of an excited state of the praseodymium(III) ion in a lanthanum trifluoride crystal at 1.5 K. The rapid oscillations correspond to the frequency shift $\delta\omega$. The envelope of the signal corresponds to $T_2^{[*]}$.

6.2. Optical Echo Experiments

In Section 6.1 we assumed for the sake of simplicity that the molecular transitions are narrow (with a width of the order of $1/T_2$). In reality, the transitions are, however, *inhomogeneously* broadened. The time decay of the polarization after a $\pi/2$-pulse is, hence, not given by equation (23) but has to be rewritten (see e.g. [52]):

$$\bar{P}(t - t_{\pi/2}) = \bar{\mu}_{01} \left[\sum_j^N \exp\{iD_j(t - t_{\pi/2})\} \right] \exp\{-(t - t_{\pi/2})/T_2\} \qquad (24)$$

where D_j characterizes the shifts of the molecular frequencies with respect to the laser frequency caused by inhomogeneity effects [see eq. (17)]. The term in the square brackets of equation (24) decays quickly due to the different molecular frequencies involved. We interpret this decay graphically by describing the polarization vector after a $\pi/2$-pulse in a *fixed* coordinate system. In such a coordinate

---

[*] In the original paper [56] the envelope corresponds to $1/2 T_2$, since effects due to the line inhomogeneity have to be taken into account. Inhomogeneity effects are, for simplicity, not included in equation (23) (see Section 6.2).

system the polarization rotates with the Larmor frequency ω_{01}. Ideally in the case of vanishing inhomogeneity, the ω_{01} frequency of all particles, i.e. molecules of the ensemble, is identical and, hence, the length of the polarization vector decays with time constant T_2. Figure 11a shows the situation for two different times τ and 2τ.
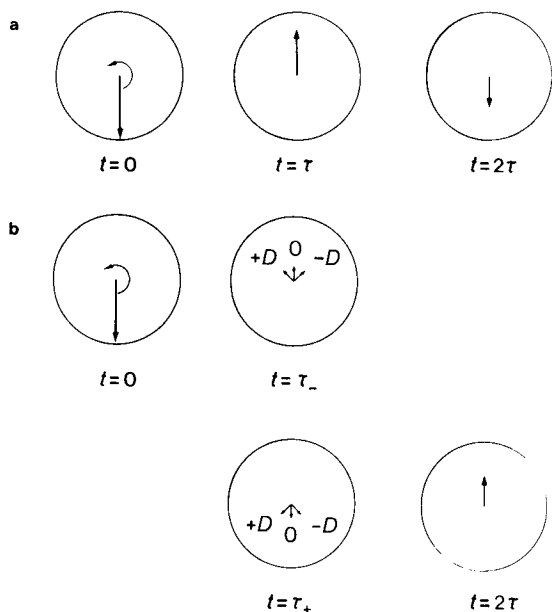

Fig. 11. a) Polarization decay (length of arrow) after a $\pi/2$-pulse. The arrow rotates at the Larmor frequency ω_{01}. The polarization executes $n+1/2$ rotations during the time interval τ and $2n+1$ during the time interval 2τ ($n=\omega_{01}\cdot t/2\pi$). The polarization decays exponentially with characteristic time T_2. b) In the presence of inhomogeneous broadening, the polarization decays faster. The polarization is symbolically composed of three different components: one with the unperturbed Larmor frequency (0) and a faster (D^+) and a slower (D^-) component. τ_- is the time immediately before and τ_+ the time immediately after the 180°-pulse. (The three arrows are all short due to the "spread out" from inhomogeneity.) After $2n+1$ rotations of the polarization the three components refocus and give rise to an echo. (The difference of half a rotation between a) and b) is due to the 180°-pulse.)

Due to the scattering of molecular frequencies in the range $\omega_{01} \pm D$ (inhomogeneous broadening), a decay of the polarization which is much faster than the "true" T_2-decay is also encountered. This is shown in Figure 11b for the time interval $0 \le t \le \tau$. For simplicity we consider only three frequency components: An unshifted component at ω_{01}, a fast component at $\omega_{01} + D$, and a slow component at $\omega_{01} - D$. If after a time τ a π-pulse is applied to the system, the slow and the fast components are interchanged as shown in Figure 11b, the slow component preceding the fast (a π-pulse corresponds to an inversion in the two-level system). If one follows the time evolution of the system after the π-pulse, the various Larmor components refocus at $t = 2\tau$ and are shifted by 180° (Fig. 11a). The polarization which refocusses at $t = 2\tau$ generates an optical echo, which can be detected in a similar way to the OFID signal. The π-pulse has the consequence that at $t = 2\tau$ the interference term of equation (24) (square brackets) is equal to unity, as is shown graphically in Figure 11b for two discrete D_j values. Equation (25) describes the decay of the refocussed polarization function, which is measured in an echo experiment.

$$\vec{P}(\pi/2,\pi,2\tau)=\vec{\mu}_{10}N\exp\{-2\tau/T_2\} \qquad (25)$$

The echo method was first introduced by *E. L. Hahn* in NMR spectroscopy[57]. The first optical echoes were measured in 1964 in ruby crystals[48] (for a survey see [58,49]).

7. Relaxation Spectroscopy in the Frequency Domain

In Section 6.2 we described methods of measuring relaxation times by transient methods in the time domain. With the aid of equation (12) relaxation times can also be measured in the frequency domain. Both methods have advantages and disadvantages and are, in many respects, complementary. In the following we summarize their main differences.

a) Experiments in the frequency domain are difficult to perform for long relaxation times because they require both high frequency resolution and high frequency stability. Practical limits at present are ca. 10^{-4} cm^{-1} (1 MHz)[59,60]. For long relaxation times, FID and echo methods are preferable.

b) Frequency domain experiments are easier at short relaxation times (5 ps $\hat{=}$ 1 cm^{-1}). This favors their application to amorphous materials which have short relaxation times, i.e. glasses and polymers[43,45,61]. For these materials transient experiments have so far, with a few exceptions[62], failed. This was mainly due to difficulties in producing sufficiently rapid pulse sequences and high enough Rabi frequencies. At the very high laser powers required, sample heating is often a problem.

c) In contrast to transient experiments, frequency domain experiments can be performed with very low laser powers and are based on a photochemical process in which the sample accumulates the experimental information. Instead of performing an experiment over a short time span under high intensity conditions, the experiments can be extended over a longer time period with correspondingly lower laser intensities. This is principally important for low temperature experiments where sample heating has to be avoided.

d) Due to their advantages at very short relaxation times, frequency experiments are extremely useful for studies of phonon states, which are characterized by very short relaxation times[63,64].

e) A difficulty which arises with experiments in the frequency domain is the interpretation of the line shapes. Line shapes are not always Lorentzian as predicted by simple theories of relaxation. Spectral diffusion processes often have to be considered in addition to straight forward relaxation processes[65]. In the latter case the complementary use of time- and frequency-domain experiments is advantageous.

7.1. The Method of Fluorescence Line Narrowing

As mentioned in Section 4, in the solid state optical line widths are limited by inhomogeneity effects. Figure 9 shows symbolically that sites with different microstructures lead to line broadening. These broadening effects occur in both crystalline and amorphous materials; they are,

Angew. Chem. Int. Ed. Engl. 23 (1984) 113–140

121

however, much more dominant for amorphous systems, leading to line widths of the order of several 100 cm^{-1}. The first investigations suppressing inhomogeneity effects were echo experiments on ruby performed by *Hartmann* et al.[48]. The first fluorescence line narrowing (FLN) experiments were also carried out on ruby by *Szabo*[66], who measured a homogeneous line width of 2×10^{-3} cm^{-1}. The FLN method was subsequently successfully applied to organic systems by *Personov* et al.[63] and to inorganic systems by *Riseberg*[67]. In the context of this article, we do not intend to give an exhaustive review of the FLN work; it is of relevance, however, that the optical spectroscopy of glasses has received new impulses through the introduction of FLN spectroscopy[63,67,68]. The advantage of the FLN method is its high resolution capability; its disadvantage is its off-resonance character. Usually one excites the 0-0 transition via laser stimulation and monitors the fluorescence of vibronic sidebands. Since the vibrational sidebands do not always have a full correlation with the 0-0 band, some line shape information is lost if only the sidebands are detected (see Section 12). Exceptions to these spectroscopic limitations are excited states with long lifetimes (phosphorescence line narrowing)[56,66,69]. In this case the optical spectrum can also be observed at the resonant laser frequency by gating methods (see dotted arrow in Fig. 12). In principle, this gating method can also be applied for short lived singlet states (10^{-8} s). Fast gating experiments are, however, difficult and to date the method has found no practical application.
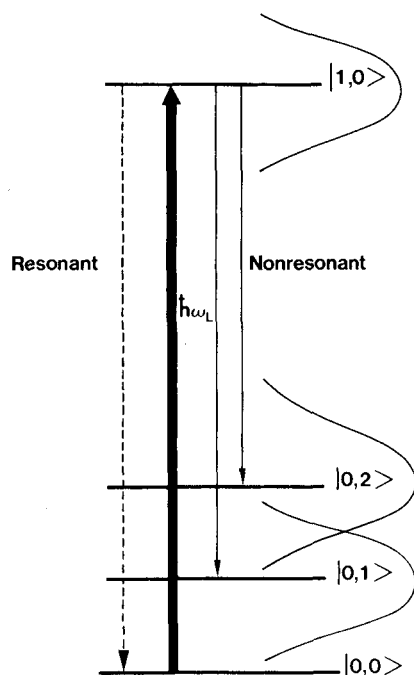

Fig. 12. Energy level scheme of a molecule with resonant and non-resonant fluorescence transitions. The symbol i,j characterizes the i-th electronic and the j-th vibrational level.

7.2. Spectral Hole Burning

The hole burning method was first introduced to NMR spectroscopy by *Bloembergen* et al.[70]. By saturating a two-

level system, a hole can be "burned" in an inhomogeously broadened NMR line. The linewidth of the hole is, within a factor of two (vide infra), of the order of $1/T_2$.

Optical hole burning experiments were first performed in the gas phase[71]. The first experiment in the solid state was carried out on ruby by *Szabo*[72].

Transient NMR hole burning is a rather straightforward experiment because of the long T_1-times, which characterize the population decay following partial line saturation. A transient hole burning experiment has to be performed within a T_1-period, which, for nuclei, can be of the order of seconds to hours. Typical optical T_1-times for allowed optical transitions are of the order of 10^{-8} s; transient hole burning experiments in the optical domain are therefore difficult. *Szabo*'s experiment[72] was performed with a comparatively long-lived, forbidden transition in ruby (R_1 band).

Photochemical and *photophysical* hole burning experiments exhibit strong analogies to transient hole burning, but circumvent the difficulty which arises at short T_1-values. Figure 13 gives an extended two-level scheme characterizing both the photochemical and the photophysical experiments. Besides the states $|\Psi_0\rangle = |R\rangle$ and $|\Psi_1\rangle = |I\rangle$ discussed so far, one has to consider a photochemical product state $|P\rangle$ which is populated with quantum yield Φ. The absorption of n quanta transforms nΦ molecules into the photochemically or photophysically modified state $|P\rangle$. This process leads to a depletion of the ground-state and thus to a permanent hole in the absorption band, provided a back reaction from $|P\rangle$ to $|R\rangle$ is forbidden or infinitely slow. The first experiments on photochemical and photophysical hole burning were published in 1974 by *Rebane* and *Personov* and their respective groups[3,4]. The high resolution of the hole burning experiments was demonstrated two years later in 1976[73,74]. Applications of hole burning to the spectroscopy of glasses were first reported in 1976[42,46].
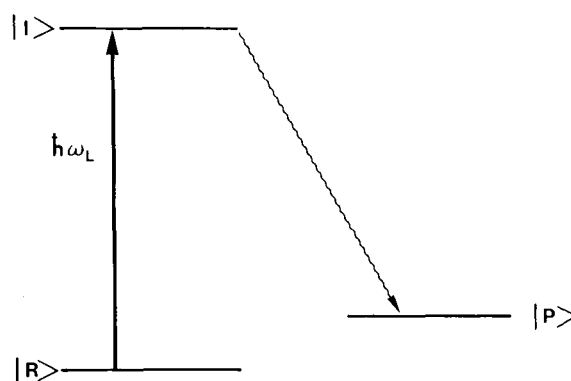

Fig. 13. Energy level scheme for the photochemistry of the hole burning process. $|R\rangle$ is the reactant state, $|P\rangle$ the product state, and $|I\rangle$ an intermediate state (for example the S$_1$ state).

With the aid of a few examples the difference between photochemical hole burning (PHB) and photophysical hole burning (non-photochemical hole burning, NPHB) will next be described.

In a typical PHB experiment the photoreactive molecules undergo photochemical changes, i.e. the absorption of the photoproduct is, in most cases, spectroscopically

122

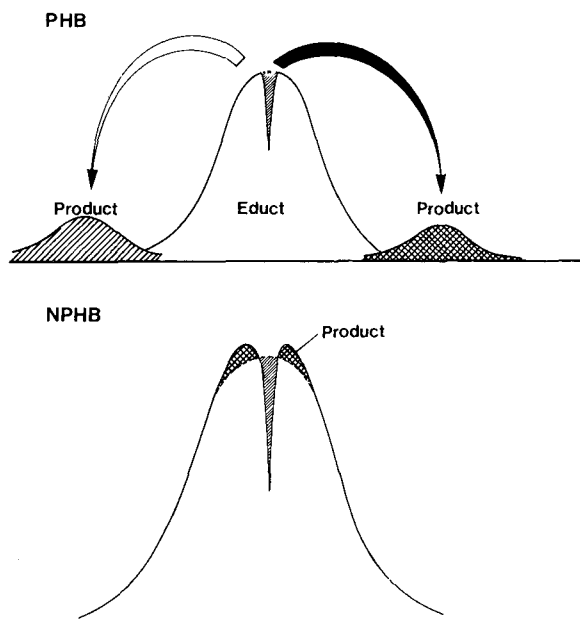*Angew. Chem. Int. Ed. Engl. 23 (1984) 113–140*

PHB

NPHB

Fig. 14. Spectral distribution of the photoproduct after photochemical (PHB) and photophysical (NPHB) hole burning: The hole in the absorption band is clearly discernible.

well separated from that of the original absorption (educt). The new absorption can be both blue- and red-shifted (Fig. 14). Examples of reversible PHB processes are proton transfer in metal-free phthalocyanine and in porphin[74] or configurational changes of hydrogen bonds[61]. An example of irreversible PHB photochemistry with large photochromic shift is the two-photon photochemistry of dimethyl-*s*-tetrazine[73,75]. In the latter case, the molecule dissociates into fragments which absorb in the UV range of the spectrum. In all these cases a photoproduct $|P\rangle$ can be defined whose optical absorption is rather different from the spectrum of the pristine molecule. There are also photoactive systems at the border area between transient hole burning and photochemical hole burning; for example, color centers[60]. For such systems the "photochemistry" arises from a reversible, light-induced electron tunneling process. (The back-reaction in the dark usually has a time constant of the order of tens of minutes.)
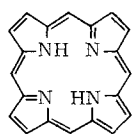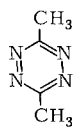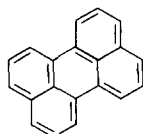
Porphin   Dimethyl-   Perylene
                 s-tetrazine

The NPHB method usually photochemically modifies the molecule-matrix interaction. As "photoactive" molecules usually species such as pyrene[4] or tetracene[43,46] are used, which, under normal conditions, are quite photostable. The light-induced changes of the optical properties depend, by definition, upon properties of the matrix. Matrices which form hydrogen bonds (e.g. ethanol-methanol glasses) seem to be suitable for this kind of photochemistry, whereas saturated hydrocarbons (e.g. *n*-alkanes) seem

to be inapt for appropriate host-guest rearrangements. A spectroscopic selection criterion which distinguishes photochemical and photophysical hole burning processes is the position of the absorption of the photoproduct, which for the latter lies very close to the energy of the laser performing the site selection[43]. Therefore, the physical variant can be interpreted as a process which redistributes molecular absorbers within the inhomogeneous band profile. On a microscopic basis this can be envisaged as a process which changes a given molecule-matrix configuration into another which absorbs at a different frequency. Recently NPHB processes have also been observed in amorphous aromatic guest-host systems[76] (see Section 13). It should, finally, be mentioned that NPHB processes have also been observed in the IR spectral range (≈ 1000 cm^{-1})[77].

8. Photochemical Hole Burning: Mechanistic Aspects

In this section we discuss various basic mechanistic aspects underlying hole burning photochemistry. We argue that hole burning photochemistry is a special kind of photochemistry, fulfilling the criterion of "zero-phonon photochemistry"[61]; the latter criterion eliminates many known photochromic systems as good candidates for hole burning.

In Section 2 we discussed the criterion for the appearance of narrow zero-phonon lines in considerable detail, and saw that weak electron-phonon coupling (i.e. small S-values) was the main condition for observing intense zero-phonon lines [(eq. (8)]. A necessary condition for weak phonon coupling was a small change of the equilibrium configuration (q_{i0}) of the lattice in the excited state. Photoreactive molecules, however, are characterized by large changes of their molecular geometry along a reaction coordinate Q (Fig. 15a)[*]. These large changes in the reaction coordinate lead to large changes in the equilibrium positions of the lattice q_{i0}.

In general, photoreactive molecules therefore show strong electron-phonon coupling. The spectra of photoreactive molecules are therefore, on the whole, characterized by broad spectral bands and large Stokes-shifts. Arguments along these lines led to the postulate of proton-transfer processes in the excited state from an analysis of the corresponding molecular spectra[78,79].

From these arguments one can conclude that PHB processes require the existence of mutually exclusive conditions; namely photoreactivity on the one hand and sharp spectral lines on the other. However, for two photochemical reaction schemes, under which most known photoreactions can be categorized, both criteria are fulfilled simultaneously. Figure 15b shows what is termed "slow photochemistry". In this case the photoreactive state is not the site-selected state itself, but a third state. This state is mostly populated via radiationless transitions; it can be a triplet state (level crossing in Fig. 15b). The proton-transfer

[*] Q denotes an internal molecular coordinate, whereas q is used throughout this article to denote lattice coordinates.

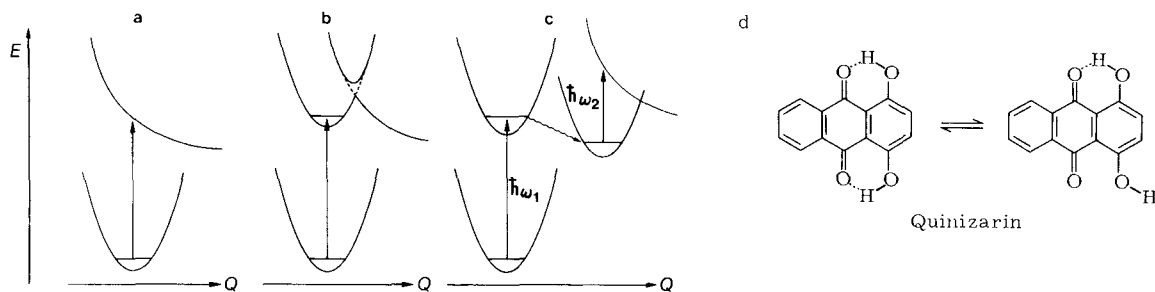*Angew. Chem. Int. Ed. Engl. 23 (1984) 113-140*

123

Fig. 15. a)—c) Photochemical model based on a configuration coordinate description of the photochemical process (see text). Q symbolizes an intramolecular coordinate. d) Reaction scheme for the proton transfer in quinizarin.

photochemistry of quinizarin (Fig. 15d) and the photochemistry of H_2-phthalocyanine and -porphin fall into this category. Even photophysical hole burning (NPHB) can be subsumed under this category. In the latter case it seems that the photochemical product state is reached via tunneling processes (see Section 13).

A second possible scheme is based on a *two-photon process*, as observed in the case of dimethyl-s-tetrazine[80]. Here, the first photon makes a site-selective transition into a photochemically inactive state, which undergoes relaxation to an intermediate state. The subsequent absorption of a second photon leads to a reactive state which initiates the photochemistry. The intermediate state has to be long-lived to achieve an acceptable quantum yield. Its spectroscopic properties are irrelevant for the hole burning process, whose site selection mechanism occurs during the transition $\Psi_1 \leftarrow \Psi_0$. Figure 15c shows the reaction scheme for a two-photon process[81]. In general, two-photon processes are desirable for technical applications such as optical memories and holographic photochemical applications. The technical advantage is that the first photon acts as a sensitizer, whereas the second photon initiates the irreversible information storage processes (see Section 15).

An important aspect of PHB photochemistry is the role played by the host lattice, which can, for example, cause activation barriers on the energy surfaces, thereby stabilizing various photochemical states[82]. Hence, at low temper-

atures, certain photochemical pathways may be inaccessible due to activation barriers which cannot be overcome by thermal energy. Such a case has been investigated using the dye molecule quinizarin as the photoreactive system[83]. The molecule undergoes light-induced proton transfer in which an intramolecular hydrogen bond can be opened or closed, depending on the wavelength of irradiation. The experimental results for the back transfer reaction of the proton indicate that the reaction can only occur in an excited phonon state of the lattice. The phonon excitations provide the energy to overcome the barrier of several 10 cm^{-1}, as shown in Figure 16. It should be noted that the phonon excitations needed to overcome the reaction barrier are "automatically" provided by Franck-Condon excitation of molecule-lattice states, as long as the molecule exhibits reasonably strong electron-phonon coupling. The forward reaction in which the hydrogen bond is opened is believed to occur via a low lying triplet state. We are not aware of any other examples of "phonon selective" photochemical reactions at low temperatures; however, no systematic studies of photochemical reactions have been performed at very low temperatures.

9. Model Calculations of Photochemical Hole Burning in Organic Glasses

9.1. Line Shape Equations for Photochemical Hole Spectra

The three-level system shown in Figure 13 accounts for many characteristic features of the hole burning process: The photochemical process leads from the initial state $|R\rangle$ via an intermediate state $|I\rangle$ to the final photoproduct state $|P\rangle$. The excitation energies $\hbar\omega'$ of the initial state are scattered around a center of energy $\hbar\omega_0$ with the width Γ, due to a variation of the D values about D_0 [eq. (17)]:

$$\frac{N(\omega')}{N_0} \equiv \rho(\omega') = 2\sqrt{\frac{\ln 2}{\pi}} \cdot \frac{1}{\Gamma} \exp\left\{ -\frac{4(\omega'-\omega_0)^2 \ln 2}{\Gamma^2} \right\} \tag{26}$$

$N(\omega')/N_0$ is the fraction of molecules which absorb in the frequency interval $d\omega'$ centered at ω'. In order to calculate the PHB line shape, the number of molecules at ω' after laser irradiation at ω_L must first be calculated.

It is important to note that a molecule which is centered at ω' absorbs at the laser frequency ω_L via two different processes: through the wings of its zero-phonon line z and through its phonon sideband p (Figs. 17 and 4). The transi-
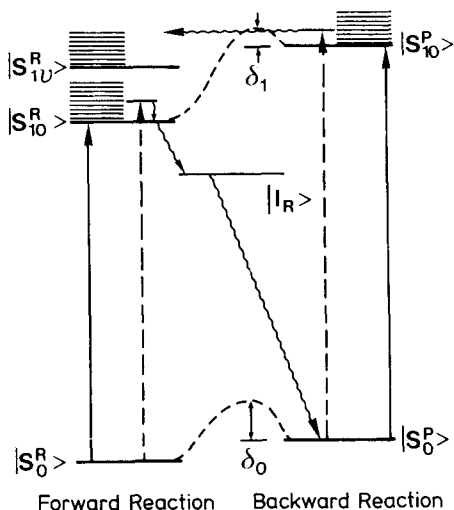

Fig. 16. Energy level scheme for the photoreactive state of quinizarin. $|I_R\rangle$ is a state of a reactive intermediate (most likely triplet); δ_0 and δ_1 symbolize reaction barriers in the ground and excited states, respectively.
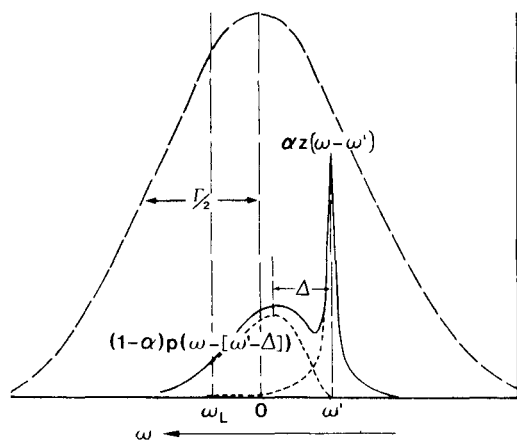
Fig. 17. Inhomogeneous distribution with a half width of Γ (full width at half height; FWHH) and spectral line shape profile of a molecule absorbing at frequency ω': z is the zero-phonon line, p the phonon sideband, ω_L: laser frequency. α: Debye-Waller factor. Δ: half the Stokes-shift. (The zero of the frequency scale corresponds to the frequency ω_0.)

tion probability per time unit can therefore be expressed as the sum of two terms

$$W(\omega_L, \omega') = \frac{\sigma I}{\hbar \omega_L} \{\alpha z(\omega_L - \omega') + (1-\alpha)p(\omega_L - \omega' - \Delta)\} \quad (27)$$

where σ is the absorption cross-section integrated over the frequency space, and $I/\hbar\omega_L$ is the number of incident photons per unit time and unit area. If Φ is the photochemical quantum yield, the change in the relative number of molecules $d\rho$ per time unit dt is given by

$$d\rho = \rho(\omega')\Phi\,W(\omega_L, \omega')\,dt$$

After integration we obtain

$$\rho_\tau(\omega') = \rho_0(\omega')\exp\{-W(\omega_L, \omega')\Phi \cdot \tau\} \quad (28)$$

where τ is the burning time.

A convolution of ρ_τ and the line profile $\alpha z(\omega - \omega') + (1-\alpha)p(\omega - \omega' - \Delta)$ affords the photochemically modified absorption spectrum $A_\tau(\omega)$.

$$A_\tau(\omega) = \sigma \int_{-\infty}^{+\infty} \rho_\tau(\omega')\{\alpha z(\omega - \omega') + (1-\alpha)p(\omega - \omega' - \Delta)\}\,d\omega' \quad (29)$$

The difference $A_0(\omega) - A_\tau(\omega)$ describes the photochemical change in the spectrum, which we refer to as photochemical hole spectrum $L_\tau(\omega)$:

$$L_\tau(\omega) \equiv A_0 - A_\tau = A_0(\omega) - \sigma \int_{-\infty}^{+\infty} \rho_0(\omega')\exp\left\{-\sigma\cdot\Phi\frac{I}{\hbar\omega_L}\tau[\alpha z(\omega_L - \omega') + (1-\alpha)p(\omega_L - \omega' - \Delta)]\right\}\{\alpha z(\omega - \omega') + (1-\alpha)p(\omega - \omega' - \Delta)\}\,d\omega' \quad (30)$$

Since z is a function which is narrow compared to ρ and p, eq. (30) can be resolved into four terms which permit a quite straightforward interpretation (Fig. 18)[84]:

$$zz(\omega) = \sigma\alpha\rho_0(\omega_L)\left\{1 - \int_{-\infty}^{+\infty}\exp\left\{-\frac{\alpha\sigma I\Phi\tau}{\hbar\omega_L}z(\omega_L - \omega')\right\}z(\omega - \omega')\,d\omega'\right\} \quad (31)$$

where $zz(\omega)$ is the narrow zero-phonon hole, whose shape depends on experimental parameters such as laser intensity I and burning time τ.
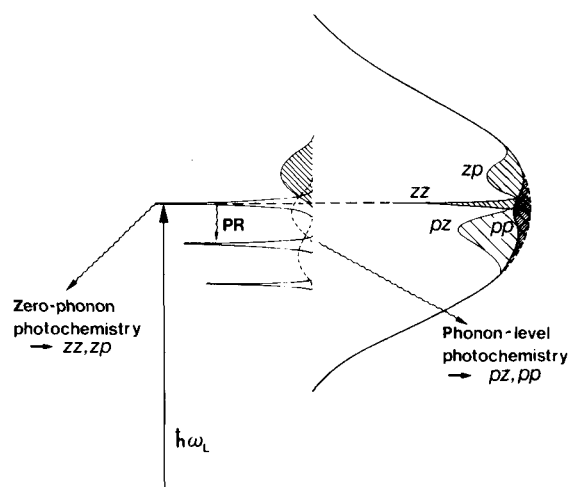

Fig. 18. Graphical scheme representing the four contributions to a photochemically burned hole zz, zp, pz, and pp. PR: phonon relaxation (see text).

The molecules whose electronic energy is centered at the zero-phonon line $zz(\omega)$ give rise to a phonon sideband absorption, which in turn gives rise to a broad hole on the short wavelength side of the zero-phonon hole. This broad hole is called the direct phonon sidehole, because it is a true satellite of the zero-phonon line:

$$zp(\omega) = \sigma(1-\alpha)p(\omega - \omega_L - \Delta)\cdot N_z(I, \tau) \quad (32)$$

The line shape of zp is determined solely by the phonon spectrum p. $N_z(I, \tau)$ is the relative number of molecules which have been changed photochemically by zero-phonon absorption:

$$N_z(I, \tau) = \rho_0(\omega_L)\left\{1 - \exp\left[\frac{-\sigma\alpha I\Phi\tau}{\hbar\omega_L\gamma_h}\right]\right\}\gamma_h \quad (33)$$

$N_z(I, \tau)$ is proportional to the homogeneous line width γ_h. The exponent in equation (33) defines a bleaching time τ_b for the zero-phonon line[84]:

$$\tau_B = \gamma_h \left/ \frac{I\Phi\alpha\sigma}{\hbar\omega_L}\right. \quad (34)$$

τ_b is rather short for low temperatures (≈ 1 K), since γ_h is small. It should, however, be noted that γ_h may increase rapidly with increasing temperature (see Section 10).

Figure 18 shows that in addition to molecules absorbing in their zero-phonon lines, one has to consider molecules with electronic energies lower than $\hbar\omega_L$. These absorb at the laser frequency via their phonon sidebands. This process creates a broad hole at energies lower than $\hbar\omega_L$, which is basically characterized by the line shape of the phonon sideband

Angew. Chem. Int. Ed. Engl. 23 (1984) 113–140

125

$$pz(\omega) = \sigma\alpha\rho_0(\omega)\left\{1 - \exp\left[-\sigma(1-\alpha)\frac{I}{\hbar\omega_L}\Phi\tau p(\omega_L-\omega-\Delta)\right]\right\} \quad (35)$$

where $pz(\omega)$ depends on the parameters I and τ used in the experiment. This dependency causes a strong asymmetry in the hole burning line shape as the total light dose $I\cdot\tau$ increases (Fig. 19). We call $pz(\omega)$ a *pseudo-phonon hole,* since
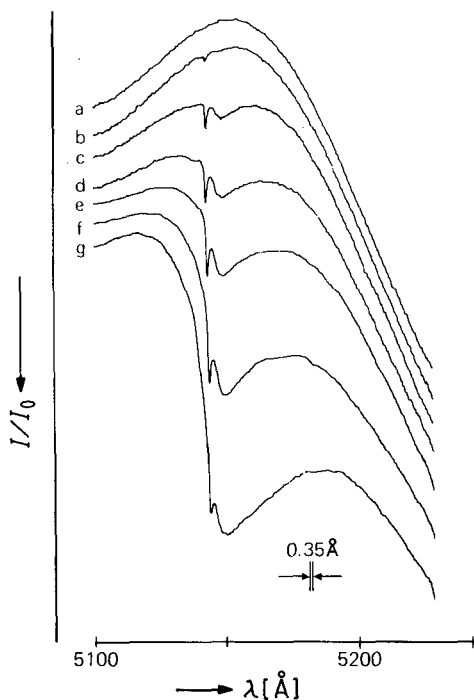

Fig. 19. Growth of a photochemical hole as a function of integrated irradiation time. Quinizarin in ethanol-methanol glass (3 :1). a) Spectrum prior to irradiation, b) after 1 s, c) after 6 s, d) after 16 s, e) after 1 min, f) after 5 min, and g) after 32 min irradiation time (Argon ion laser, 7 mW/cm²; $T = 1.8$ K).

this term does not represent a real phonon sideband belonging to a zero-phonon origin (it is rather a convolution of zero-phonon lines). Finally, the molecules which constitute the pseudo-phonon hole have their own phonon wings. This gives rise to a phonon-phonon term:

$$pp(\omega) = \sigma(1-\alpha)\int_{-\infty}^{+\infty}\rho_0(\omega')\left\{1-\exp\left[-\frac{\sigma I}{\hbar\omega_L}\Phi\tau(1-\alpha)p(\omega_L-\omega'-\Delta)\right]\right\}p(\omega-\omega'-\Delta)\,d\omega' \quad (36)$$

Whereas zp is on the short wavelength side of ω_L and pz is on its long wavelength side, pp has contributions on both sides of ω_L and, for low radiation dose, is symmetric with respect to ω_L (see Section 9.2). For small electron-phonon couplings pp is of minor importance, since the small quantity $(1-\alpha)$ appears both in front of the integral and in the exponent of equation (36).

9.2. Limiting Cases: Short Burning Time Limit

If the burning time τ is considerably shorter than τ_b, the exponent of equation (31) can be expanded into a power series. Neglecting higher terms, the line shape of the zero-phonon hole can then be written as

$$zz(\omega) = \frac{I\cdot\tau}{\hbar\omega_L}\sigma^2\alpha^2\Phi\rho_0(\omega_L)\int_{-\infty}^{+\infty}z(\omega_L-\omega')z(\omega-\omega')\,d\omega'; \quad \tau\ll\tau_b \quad (37)$$

For most practical cases, $z(\omega)$ is Lorentzian

$$z(\omega) = \frac{\gamma_h}{2\pi}\frac{1}{(\omega-\omega')^2+\gamma_h^2/4} \quad (38)$$

In this case the convolution integral [eq. (37)] can be solved, giving

$$zz(\omega) = \frac{I\cdot\tau}{\hbar\omega_L}\sigma^2\alpha^2\Phi\rho_0(\omega_L)\frac{\gamma_h}{\pi}\frac{1}{(\omega-\omega_L)^2+\gamma_h^2} \quad (39)$$

Equation (39) is also characterized by a Lorentzian line shape; however, with a line width of $2\gamma_h$. The short burning time limit enables one to interpret line widths in terms of the pertinent relaxation times. Equation (37) further predicts a linear growth of the zero-phonon hole with irradiation time τ.

From equations (35) and (36) it can also be concluded that for $\tau\ll\tau_b$ the pseudo-phonon hole and the direct phonon hole have identical shape and depth. $L_\tau(\omega)$ is therefore completely symmetric with respect to the laser frequency ω_L[64].

9.3. Limiting Cases: Photochemical Saturation Limit

With increasing irradiation dose $I\cdot\tau$, photochemical reactions at the center of the line gradually come to a halt because most photoactive molecules have already been converted. Consequently, photochemical reactions shift increasingly to the wings of the line leading to a line broadening, termed photochemical saturation broadening (see Section 9.4). For $\tau\gg\tau_b$, the term N_z in equation (33) does not increase much. In the range of the pseudo-phonon hole, however, the photochemical reactions still progress. This is because many more molecules absorb in the area of the broad pseudo-phonon wing compared to the narrow range of the zero-phonon hole.

The hole spectrum therefore shows a non-linear growth rate (Fig. 19). These considerations make it evident that for a determination of α it is not sufficient to measure the relative intensity of the zero-phonon hole given by equation (7). Instead, a complete computer simulation has to be performed[64]. Only for times $\tau\ll\tau_b$ is the relative area of the zero-phonon hole given by α^2.

9.4. Hole Width and Laser Burning Time

The line width of the zero-phonon hole as a function of τ (or I) can be calculated analytically only for the limiting cases $\tau\ll\tau_b$ and $\tau\gg\tau_b$ using equation (31). As $\tau\to0$, the line width approaches $2\gamma_h$ linearly[85]. For $\tau\gg\tau_b$ the exponen-

126

Angew. Chem. Int. Ed. Engl. 23 (1984) 113–140

tial factor in equation (31) can be omitted from the integral, since it is a function which varies slowly with ω due to photochemical saturation (slow compared to z). Using this approximation, the hole width can be calculated as:

$$\gamma(\tau) = \sqrt{\frac{\alpha \sigma \Phi \gamma_h}{\pi \ln 2 \hbar \omega_L} I \cdot \tau} \qquad (40)$$

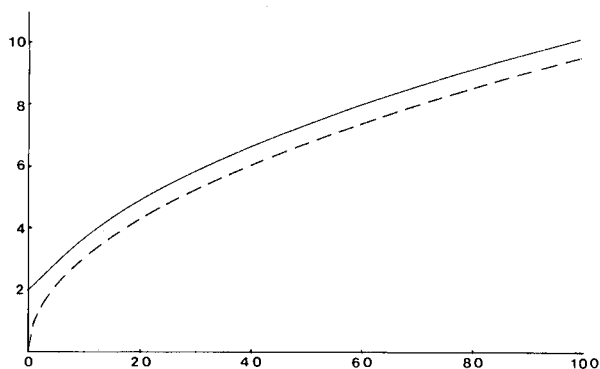The hole width increases with the square root of $I \cdot \tau$. Figure 20 shows a computer simulation of a typical saturation curve[86].

Fig. 20. Computer simulation of a photochemical bleaching curve [86] according to equation (31). Abscissa: Burning time in units of τ_b. Ordinate: Hole width in units of γ_h. The dotted line represents the asymptotic case according to equation (40).

9.5. Temperature Effects on the Emission Spectra of Photoreactive Molecules

At very low temperatures the emission spectra of photoreactive molecules in glasses exhibit a rather strange temperature behavior. In contrast to what one would expect, they do not exhibit narrow zero-phonon lines but show, instead, only broad spectra typical of phonon sidebands (Fig. 21a). At higher temperatures, however, narrow lines appear in the spectra (Fig. 21b). This rather unexpected phenomenon can be explained as follows: At low temperatures the short bleaching times lead to a rapid disappearance of molecules which absorb and emit at the laser frequency. The remaining nonresonant molecules give rise to the observed broad structures. With increasing temperatures, the bleaching time of the zero-phonon lines increases [eq. (34)] and, hence, the resonantly absorbing molecules appear in the spectrum[84]. This unconventional temperature dependence of the observed narrow zero-phonon lines is due to the bleaching effect of the photochemical system which may occur in the time scale of minutes up to several tens of minutes and, hence, may modify the observed fluorescence spectra.

9.6. Limits of the Model and Further Developments

The model which has been presented above makes assumptions which may, in some instances, not be valid. We have, for example, neglected all non-linear effects in the interaction between molecules and the laser field. This seems to be justified, if CW-lasers which operate in the
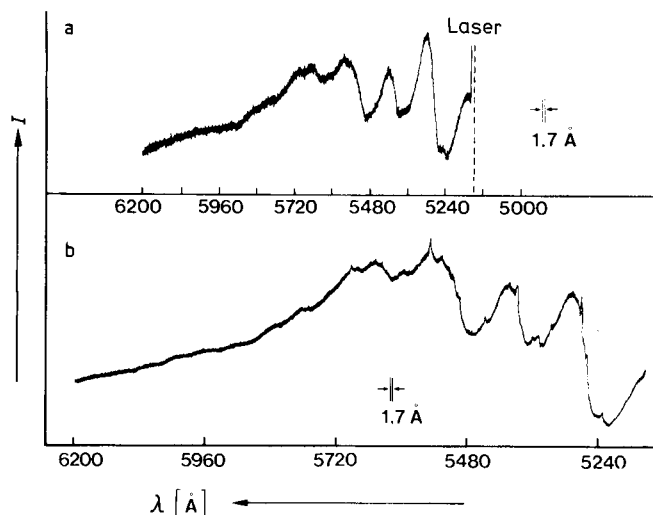

Fig. 21. Emission spectrum of quinizarin in an ethanol-methanol glass (3:1) at a) 1.8 K and b) 20 K. Excitation: Argon ion laser, 5145 Å, 7 mW/cm² [84].

mW range are used and if one investigates organic molecules in glasses which are characterized by comparatively large line widths. If, however, crystalline systems are studied using pulsed lasers, the non-linear effects may be of importance and have to be included in the theoretical treatment[87,88]. We have further assumed that no states with long lifetimes (e.g. triplet states) are involved in the photochemical cycle. Long-lived triplet states can, for example, give rise to bottlenecks and lead to accumulation of a large fraction of the molecules, thus causing non-linearities[87]. A similar effect can arise from the photochemical equilibrium between the states $|R\rangle$ and $|P\rangle$[5,88] (Fig. 13). Finally, one has to consider tunneling processes in glasses (Section 13), which can occur in the ground state and which can lead to spectral diffusion[65]. This latter effect has not been investigated yet in sufficient detail; however, it seems to have a considerable influence on the measured line widths.

Finally, it must be taken into account that in glasses all physical parameters, such as α, Φ and γ_h, are not characterized by a single, well-defined value, but by distribution functions. In consequence, the measured results may depend on the time-scale of the experiment[64].

10. Experimental Determination of Relaxation Processes in the Frequency Domain

Even in the early stages of photochemical hole burning, workers were aware of the possibility of determining relaxation times[5,73] from measurements of homogeneous line widths as defined by equations (12) and (19). By choosing appropriate experimental conditions, one can select the external parameters such that the following conditions hold

a) $1/T_2^* \ll 1/2T_1$ or b) $1/T_2^* \gg 1/2T_1$

Case a) is, for example, frequently fulfilled if the resonant state is a vibrational state. In experiments conducted using crystals at 4 K, the vibrational relaxations are, in general,

Angew. Chem. Int. Ed. Engl. 23 (1984) 113-140

127

much shorter than the pure dephasing times and hence, vibrational relaxation times can be measured down to the sub-picosecond range. Systematic experiments for various vibrational levels have been published for porphin in n-alkane matrices[89]. Figure 22 shows that there is no straightforward relation correlating the relaxation times with the vibrational energies. The measured relaxation times vary over the range 1 to 40 ps. More recent experiments have shown that the vibrational relaxation in porphin strongly depends on the host matrix and on the local molecular environment[90]. Besides the experimental determination of vibrational relaxation times, the relaxation times of purely electronic transitions can also be measured[59, 74, 91]. These experiments are more difficult, since the relaxation times involved are comparatively long and, hence, the line widths quite narrow. The laser stability required, therefore, has to be better than 10 MHz ($=3 \times 10^{-4}$ cm^{-1}). In most crystalline systems the line width at 2 K is limited by the lifetime of the excited state [eq. (10)]. (The situation is more complicated in the case of glasses, since the underlying physics is rather complex (see Section 13).) If the temperature is raised, the line width increases rapidly and one approaches the range b), in which the line width is determined by pure T_2^*-dephasing processes.
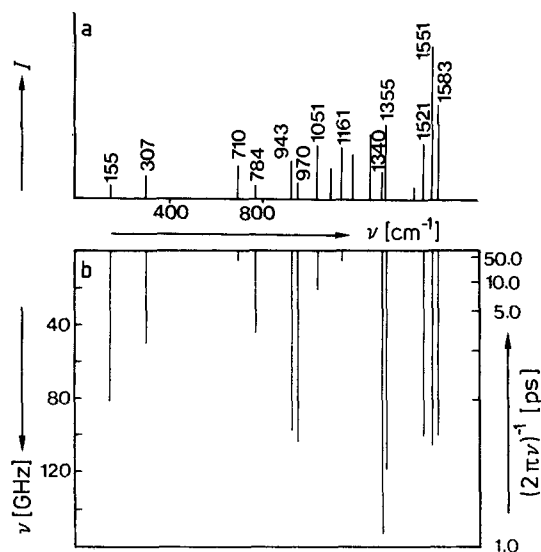
Fig. 22. Line widths of various vibronic states of porphin in n-octane [89]. a) Schematic excitation spectrum; b) corresponding line widths. v: Frequency offset from the origin.

As discussed qualitatively in Section 3, phase relaxation is due to elastic phonon scattering processes in the various electronic levels. If these scattering processes are caused by the entire Debye phonon-spectrum (non-resonant scattering), then, well below the Debye temperature Θ, the line width follows a power law proportional to T^7:

$$\gamma_h(T) - \gamma_h(0) = \gamma_2 \left(\frac{T}{\Theta}\right)^7 \qquad (41)$$

Above the Debye temperature this power law changes to a quadratic law; γ_2 is a constant and is not a function of temperature (see [23]).

If the scattering processes are mainly due to a single, localized phonon state of frequency ω_0 (such as, e.g., a libration of the molecule), it can be shown that the temperature-dependence of the linewidth γ_h is given by the thermal occupation number of the pertinent phonon state, leading to the following relation:

$$\gamma_h(T) - \gamma_h(0) = \gamma_2' \langle n(\omega_0) \rangle (\langle n(\omega_0) \rangle + 1) \qquad (42)$$

where $\langle n \rangle$ is given by equation (13). In this case one speaks of resonant phonon scattering. For $\hbar \omega_0 \ll kT$, equation (42) leads, to a good approximation, to a quadratic temperature dependence. For $\hbar \omega_0 \gg kT$, one can extrapolate to an exponential behavior $\exp(-\hbar \omega_0 / kT)$[74, 92].
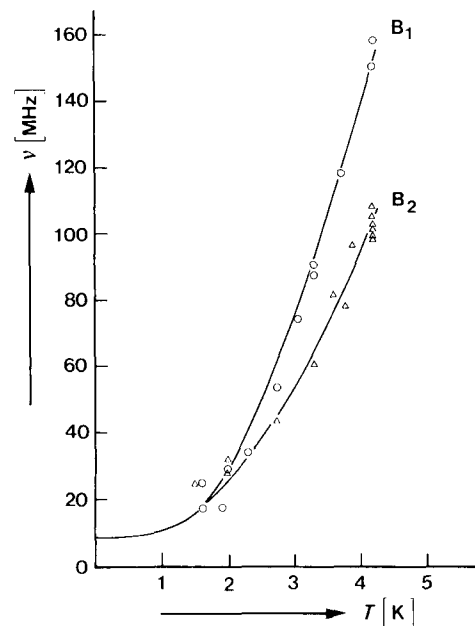
Fig. 23. Temperature dependence of the homogeneous line width of porphin in n-octane for the B_1- and B_2-sites [74].

Figure 23 shows the homogeneous line width of porphin in n-octane as a function of temperature[74]. The theoretical curves are calculated using equation (42). As $T \to 0$, the line width approaches the limiting value of 9 MHz. This corresponds to the "Heisenberg limit", in which the line width is given by the fluorescence lifetime.

The influence of local lattice vibrations can also be interpreted within the framework of the theory of the optical exchange mechanism[59, 93, 94]. Figure 24 shows the main features of the model: The optical transition between the two phonon levels shows an energy mismatch Δ with the purely electronic transition. Since the phonon states are, in thermal equilibrium, constantly created and annihilated, the optical line constantly jumps between the two transition frequencies ω and $\omega + \Delta$. This leads to a broadening which for low temperatures ($\hbar \omega_0 \gg kT$) is given by

$$\gamma_h(T) - \gamma_h(0) = 2\Delta \tau \frac{\Delta}{1+\Delta^2 \tau^2} \exp(-\hbar \omega_0 / kT) \qquad (43)$$

where τ is the lifetime of the excited phonon state. A characteristic feature of the model is the frequency shift as a function of temperature, which is given by:
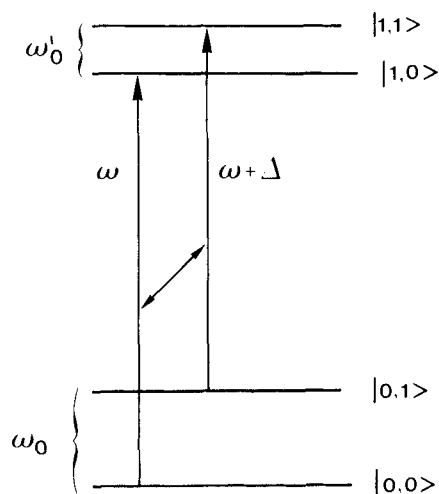
Fig. 24. Four-level scheme on which the optical exchange narrowing model is based (see text).

$$\omega(T)-\omega(0) = \frac{\Delta}{1+\Delta^2\tau^2}\exp(-\hbar\omega_0/kT) \tag{44}$$

Three cases can be distinguished[94]:

Fast exchange: $\Delta\cdot\tau \ll 1$
Slow exchange: $\Delta\cdot\tau \gg 1$
Intermediate exchange: $\Delta\cdot\tau \approx 1$

By measuring both the frequency shift and the line broadening as a function of temperature, one can determine the quantities Δ and τ as well as the energy of the associated phonon state. For porphin in n-octane the phonon energy was found to be 15 cm^{-1}; its lifetime was estimated to be 3 ps.

In the slow exchange limit the frequency shift is very small, and $\gamma_h(T)$ is independent of Δ[95].

In equations (43) and (44) τ is assumed to be independent of temperature. This assumption may be valid for phonons over a narrow temperature range. Since, however, the exchange can also occur with states other than those of phonons (e.g. TLS), τ can become temperature dependent. In this case, situations in which $\gamma_h(T)$ increases with increasing temperature and those in which it decreases with increasing temperature (optical exchange narrowing; see Section 13) can be encountered.

11. Photochemical Holes in External Fields

Due to their narrow width, photochemical holes can be regarded as excellent frequency markers which allow one to measure spectral changes of the order of a line width. These small changes would remain undetected, if one were to measure the complete broad inhomogeneous band. Hence, hole burning can be used to increase the experimental accuracy of measured line shifts by several orders of magnitude. This has been used for to measure small Zeeman and Stark shifts in doped crystals and glasses.

11.1. Zeeman Experiments

Zeeman studies of optical transitions of organic molecules were conducted in 1971 using metal porphinates[96].

These molecules have D_{4h} point group symmetry; their S_1-state is characterized by an electronic angular momentum perpendicular to the molecular plane (z-axis), which gives rise to a magnetic moment in the S_1-state. The twofold degeneracy of the S_1-state is removed in the crystal field,

Metal(II)-porphinate   Chlorin

leading to a small splitting. Due to the small splitting, the interaction between the two crystal field states is comparatively large and, therefore, the energy shift ΔE in an external magnetic field is, in case of the S_1-state, larger than the inhomogeneous band width. This large energy difference can readily be detected and allows the determination of the matrix element A characterizing the angular momentum:

$$\Delta E = -(\beta A H_z)^2/(E_2-E_1) \tag{45}$$

$$A = |\langle S_1|L_z|S_2\rangle| \tag{46}$$

Typical A values range between 4.2 and 4.3. A is an interesting quantity, because it can be calculated within the framework of structural models. Comparison with experimental data permits a convenient examination of the validity of the molecular models.
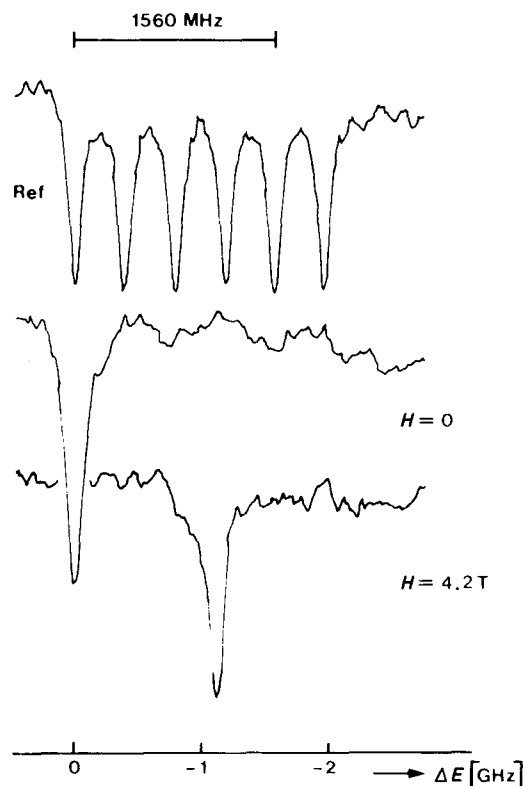

Fig. 25. Zeeman shift of a photochemical hole of porphin in n-octane [97] (see text).

Angew. Chem. Int. Ed. Engl. 23 (1984) 113–140

129

These experiments are not feasible with the free base porphin. Because the molecular symmetry is lowered from D_{4h} to D_{2h} the two levels, which were originally split by the crystal field, are now split by the molecular field and are ca. 3000 cm^{-1} apart. Equation (45) shows that the Zeeman-shift is inversely proportional to the energy splitting and, thus, one can expect Zeeman-shifts of 0.03 cm^{-1}, which is about 1/30th of the inhomogeneous line width Γ (Γ in n-alkane crystals is ca. 1 cm^{-1}). Nevertheless, by applying PHB methods it was possible to determine the Zeeman shift[97]. Figure 25 shows the results obtained using two identical samples at 2 K. One of the samples was in a superconducting coil; the other sample was used as a reference wavelength marker into which a series of holes was burnt, which were separated by the laser modes. The "master sample" had only one hole, whose shift with external magnetic field could be measured by comparing it with the hole pattern of the reference sample. Using this high precision method, it could be shown that the Λ-value is much larger for free base porphin relative to those of metal porphins. With the same method one could also perform Zeeman experiments using the two tautomers of chlorin (7,8-dihydroporphin)[98,99]. By comparison of the corresponding Zeeman-shifts in the various "sites" of the n-alkane crystal the energy difference $E_2 - E_1$ and Λ for both tautomers could be determined.

Transient optical hole burning experiments were performed using inorganic crystals. Since these crystals do not exhibit "permanent" photochemical states for the hole burning experiment, their nuclear hyperfine states were used as long-lived "hole states", marking the shifts by external fields[100,101]. If hyperfine states are used one can utilize holes as probes for RF-transitions in the spin systems and develop rather sophisticated techniques [optical detection of nuclear magnetic resonance (ODNMR) and optical detection of nuclear quadrupole resonance (ODNQR)].

11.2. Stark Experiments

Similar techniques can be used to study molecular interactions with external electric fields with vastly increased precision. Molecules without centers of inversion possess a permanent dipole moment and, hence, their transition energy changes linearly in an external electric field (linear Stark-shift). Symmetric molecules without permanent dipole moments exhibit a quadratic Stark-shift.

By evaluating these shifts, small changes in the dipole moment and in the polarizability upon electronic excitation can be measured. Frequently these methods also give some insight into the relative orientation between the guest molecule and the host crystal. Figure 26 shows the results of a Stark experiment with chlorin[102]: The hole observed exhibits splitting in an external electric field due to the inversion symmetry of the crystal. Whereas the dipole moment of chlorin only changes its absolute value (0.23 D), its photo-isomer also changes its direction. The directional change of the isomer is also "site dependent", presumably because of the strong S_1, S_2 mixing which occurs due to the small $S_1 - S_2$ energy gap.

A combination of spectral hole burning and Stark effect has also been applied to color centers in NaF[103-105]. The
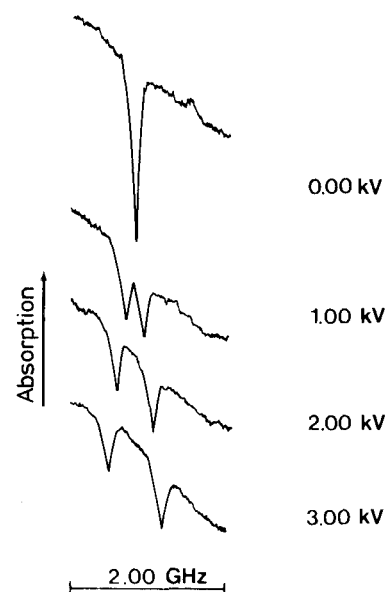

Fig. 26. Stark-shift of a photochemical hole of chlorin in n-hexane [102] (see text).

hole burning mechanism presumably involves either photo-ionization or electron tunneling in the excited state. The observed lifetimes of the corresponding photoproducts can be rather long (back tunneling to the original state). Stark experiments allow conclusions to be drawn which clarify both the symmetry and microscopic nature of the corresponding color centers.

Stark experiments in glasses are rather different from those in single crystals. Here, the external field leads mainly to broadening of the observed holes due to the geometry of the isotropic glass. From the increase in line width, the average changes in the electric (or magnetic) dipole moment can be calculated. The initial experiments were performed on the sodium salt of resorufin (Fig. 27) in
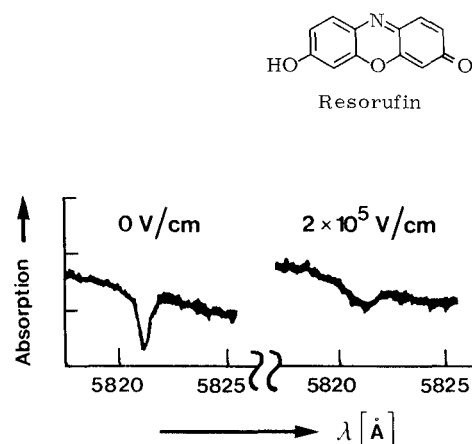

Resorufin

Fig. 27. Stark broadening of a photochemical hole of the sodium salt of resorufin in poly(methyl methacrylate) films [106].

poly(methyl methacrylate) films[106]. From these experiments one could infer a change of the dipole moment of 0.25 D upon excitation to the S_1-state. If holes are burned while an external field is applied[107,108], the hole-spectrum can subsequently be scanned by scanning the external field (Fig. 28). The maximum hole depth is achieved if the field
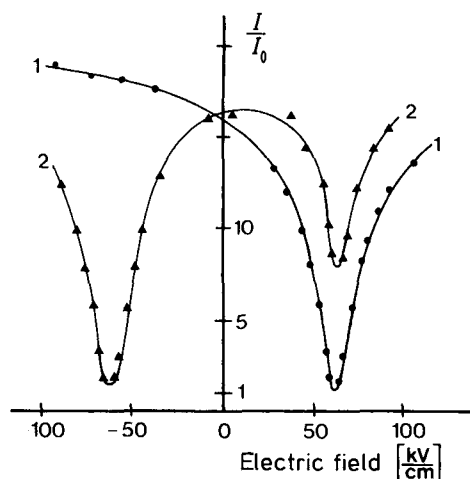
Fig. 28. Line shape of a photochemical hole as a function of the external electric field. System: Perylene in poly(vinylbutyral). 1) Hole burnt at a field of +60 kV/cm. 2) Additional hole burnt at a field of −60 kV/cm [107].

equals that at which the photochemical reaction was performed, in both magnitude *and* direction. The hole can therefore be viewed as a "memory" of the field strength and direction during the PHB photochemistry.

12. Non-Resonant Holes and Correlation Effects

Each photochemical hole burnt at the laser frequency ω_L must, in principle, appear in all other optical bands of the photoreactive molecule. A photochemical hole can therefore be investigated off-resonance at a frequency which is far removed from that of the laser. This experiment raises the question of what information can be gained using such a procedure.

Figure 29 gives an example of non-resonant hole burning: A hole was produced in the first vibrational band of 1,4-dihydroxyanthraquinone at ca. 5030 Å. As a conse-
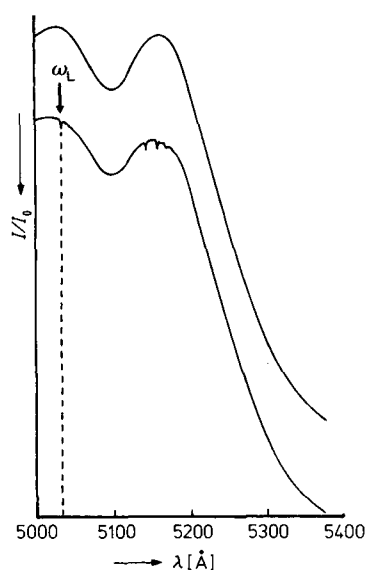

Fig. 29. Absorption spectrum of quinizarin in an ethanol-methanol glass (3 : 1) before and after hole burning at 5032 Å (1 mW/cm², T = 1.8 K). Several satellite holes appear in the 00-band of the spectrum [110].

quence, a whole sequence of holes appears in the 00-band of the molecule. The non-resonant holes in the 00-band are considerably wider than the resonant hole at frequency ω_L. Figures 30 and 31 give a more detailed view of this situation. The occurrence of multiplets of holes was first observed by *Kharlamov* et al.[109]. Multiplets appear because the difference in the frequencies of vibrational states can be smaller than the inhomogeneous band width. Hence, irradiation at ω_L leads simultaneously to photochemical holes at various sites, which appear at different frequencies in the 00-band.
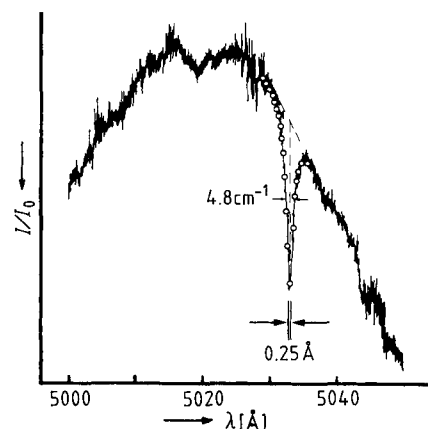

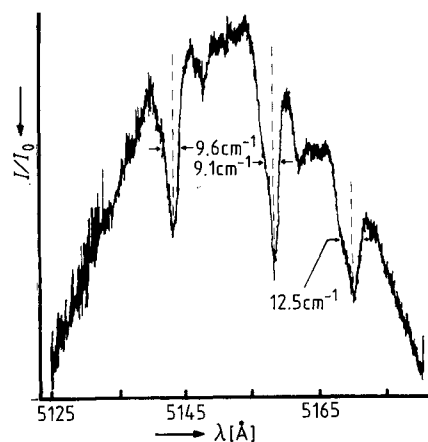Fig. 30. Enlarged section of the spectrum of Figure 29. Resonant hole [110].

Fig. 31. Enlarged section of the spectrum of Figure 29. Nonresonant satellite holes [110].

If one wants to calculate the hole shape and hole width of the relaxed holes[110], a joint probability distribution must be considered. This distribution determines the probability of detecting a photochemical process at frequency ω_2 (of the inhomogeneous 00-envelope), initiated with laser irradiation into a vibronic transition at ω_1. This is rather analogous to the problem of correlating the errors in two variables[111]. In the simplest case, the distribution function is given by a two-dimensional Gaussian distribution [eq. (47)].

$$G(\omega_1-\omega_n,\omega_2-\omega_0) = \frac{4\ln 2}{\pi\Gamma_0\Gamma_n\sqrt{1-\rho^2}}\exp\left\{-\frac{4\ln 2\cdot(\omega_1-\omega_n)^2}{\Gamma_n^2}\right\}\exp\left\{-\frac{4\ln 2\cdot[(\omega_2-\omega_0)-(\omega_1-\omega_n)\hat{S}]^2}{\Gamma_0^2(1-\rho^2)}\right\} \quad (47)$$

$\hat{S}$ is a scaling factor, which becomes 1 if the inhomogeneous widths Γ_n of the state n (here a vibrational state) and Γ_0 of the state 0 are identical. ρ Characterizes the degree of correlation:

$$\rho \equiv \frac{\langle(\omega_1-\omega_n)(\omega_2-\omega_0)\rangle}{\Gamma_n\Gamma_0}; \qquad 0 \le |\rho| \le 1 \quad (48)$$

By examining two limiting cases, the significance of ρ becomes apparent. If $\rho = 1$ complete correlation results; the second Gaussian function in equation (47) ist a δ-function and there is complete site selectivity in the non-resonant state. The widths of the non-resonant holes in this case are narrow and determined by the pertinent dephasing times. (The fluorescence from the non-resonant state is also narrow.) If the condition $\rho = 0$ holds, the second Gaussian function in equation (47) has a width of Γ_0, i.e. a state which had been site-selected in the vibrational level n will be spread over the complete inhomogeneous band characterizing the 00-transition. In the latter case no narrow holes appear at the origin. In reality, one finds the situation of intermediate correlation. Here the hole shape can be calculated by a convolution of the zero-phonon lines $z_n(\omega)$ and $z_0(\omega)$ with the corresponding inhomogeneous profiles given above can be measured. If instead of focussing on a (i.e. to a convolution of a Gaussian and Lorentzian profile). If the homogeneous line widths in the states n and 0 are small compared to the width of the non-resonant holes, the shape of the non-resonant holes is Gaussian and their widths are given by $\Gamma_0(1-\rho^2)^{1/2}$.

By measuring this width (Figs. 30 and 31), one can calculate the loss of correlation between the vibrational state considered and the electronic origin: for quinizarin, $1-\rho \approx 10^{-5}$.

This means that the vibronic transitions are highly correlated with their electronic origin. It is only because of the narrow hole width that correlation losses as small as those given above can be measured. If, instead of focussing on a vibrational state n, one focussed on a different electronic state, for amorphous hosts, a vanishing correlation occurs as a rule. However, there is a possibility in crystalline materials that a certain degree of correlation may still exist even for different electronic states. Experiments probing the degree of correlation can therefore be looked upon as experiments which shed light on the role played by the solvent in optical excitation processes.

To understand the correlation phenomena discussed here, one has to consider a microscopic model. *Gorokhovskii* and *Kikas*[112] assumed that the inhomogeneity not only affects the various electronic levels, but also independently the vibrational levels. Figure 32 reflects this argument for an energy level scheme. If one excites into a vibrational level, two different sites are excited which have slightly different vibrational energies, but which, nevertheless, absorb at the same frequency ω_L. In the 00-transition both sites differ in frequency by the difference of their vibrational energies. If instead of two sites one has a complete

site distribution, the above argument leads to an inhomogeneous broadening of the vibrational frequencies. This broadening is, on a relative scale, comparable to the inhomogeneous broadening of electronic levels. Besides correlation effects, using non-resonant holes, one can study the vibrational frequencies of photoactive molecules in the excited state[109, 113]. Even in glasses, these frequencies can be studied with great accuracy. These experiments complement FLN techniques which allow the determination of ground state frequencies. By using both PHB- and FLN techniques vibrational frequency changes upon electronic excitation of molecular states can therefore be measured with great accuracy.
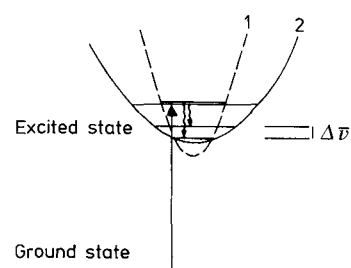

Fig. 32. Microscopic model describing the observed vibrational inhomogeneities. Sites 1) and 2) have slightly different vibrational energies.

13. Amorphous Solids

In 1976 the first fluorescence line narrowing (FLN) experiments were performed using inorganic glasses doped with paramagnetic ions and it was observed that optical properties in crystalline systems were quite different from those in amorphous solids[114]. For example, the homogeneous line width did not increase with T^7 (see Section 10), but increased with a lower temperature exponent. Similar observations were made for ESR and NMR experiments[115-117]. In addition, the observation was made that the homogeneous line width in glasses was much larger than that in crystals[114, 118, 119].

At first, these results came as a surprise, because it was known that the Debye model could be applied to glasses, and that optical line widths were mainly determined by elastic phonon scattering. A comparison of these new findings with results obtained from experiments on organic glasses created some new aspects. FLN experiments could only partly be evaluated due to the above discussed difficulties concerning correlation effects. Most new aspects therefore came from hole burning experiments[11, 45, 46, 61, 106, 119] (see also [5]). Even the initial experiments indicated that the optical line widths in organic glasses were larger than those typical of inorganic glasses[46]. The measured hole widths were, even at 2 K, almost a wavenumber; this was an important fact, which had to be taken into account by theoretical considerations. As we have seen in Section 3, the homogeneous line width as $T \to 0$ is given by the "Heisenberg-limit", i.e. by the lifetime

132

Angew. Chem. Int. Ed. Engl. 23 (1984) 113–140

of the excited state [eq. (10)]. Hole burning experiments, however, showed deviations from the Heisenberg-limit of up to three orders of magnitude, and there was considerable discussion as to the possibility of a residual line width as $T \to 0$. This discussion was interesting, because some systems, like porphin, allowed an extrapolation to the "Heisenberg-limit" as $T \to 0$[120-122] (with a power law $T^{1.33}$). Similar results were obtained for chlorin in polymer films[123]. The various conflicting data showing different temperature exponents and different residual line widths stimulated various theoretical model calculations[44,46,119,124,125-129]. One of the salient points of most models was a coupling mechanism of the dye probe molecules to the double-well potentials of the glassy state (Fig. 33a). If coupling to a single double well potential is considered, one has to deal with a total of four levels (Fig. 33b). It is of importance that a glass is, by definition, a system which is not in thermodynamic equilibrium; it has a residual entropy at $T = 0$. Therefore, even at this temperature relaxation processes can occur via phonon emission (Fig. 33b), and can contribute to the line width. For a final assessment of this situation, however, a complete knowledge of the microscopic glass parameters would be necessary: Such parameters are barrier heights and energy values of the TLS levels, coupling matrix elements, veclocities of sound, etc. With these parameters still undetermined, the question as to the "true" homogeneous line width has no definite answer, yet.
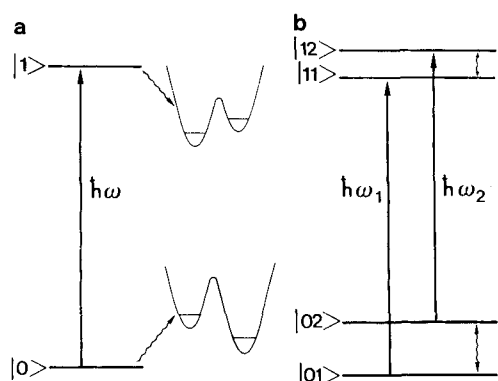
Fig. 33. a) Model describing the coupling of an optical transition to the tunneling potentials of a glass. b) Generalized level scheme. The symbols |0⟩ and |1⟩ correspond to the electronic excitations. The symbols |01⟩, |02⟩ and |11⟩, |12⟩ symbolize the corresponding tunneling states in the ground and excited states, respectively.

New theoretical aspects were introduced by considering "fractal dimensions"[130]. We can visualize this new concept by constructing a glass through areas of solid material, which are statistically interrupted by areas of "free volume". The general topological properties of such a composite system can, in general, not always be described by a three-dimensional model. The topology could, for example, be mainly two-dimensional with some "local defects" pointing into the third dimension. This is important for calculations of the phonon density of states, which can be different from the usual situation encountered in a three-dimensional lattice. The new dimensionality is smaller than three, yet, larger than two: One can speak of "fractal dimensions", whose elementary excitations are termed

"fractons". If the TLS-levels are coupled to fractons, instead of to phonons, one can expect different power laws for the optical line width due to the different density of states[131]. Under certain conditions (percolating network, dipole-quadrupole coupling) one arrives at a power law of $T^{1.33}$. There is, however, a limitation to the applicability of fracton excitations. The theory can only be applied above a critical temperature T_c. At the critical temperature the average phonon wavelength is of the length of a structural domain. Therefore, one has to consider domain excitations for $T > T_c$ and thermal phonon excitations for $T < T_c$. In the latter case the domain structure is of little relevance and a simple Debye spectrum can be assumed. A temperature law of $T^{1.33}$ has also been obtained by other theoretical approaches[129,134].

The concept of two-level systems also leads to further, interesting consequences (Fig. 33b): Since the TLS-splitting is, in general, different in the ground and excited states, the transitions 1 and 2 of the four-level scheme are non-degenerate. At low temperatures this difference in TLS-splittings contributes to the optical line width. It can be assumed that, at high temperatures, the relaxation pathways shown in Figure 33b are so efficient that optical "exchange narrowing" takes place. If one were to assume that the relaxation processes slow down at low temperatures, an increase of the line width with decreasing temperature would be expected, as is shown in Figure 34[132]. Line broadening of this type with decreasing temperature is well known in NMR spectroscopy; however, to our knowledge no comparable results have been obtained in the optical domain, other than the preliminary data on amorphous polymers.

The discovery of irreversible contributions to the optical line width of dye molecules in glasses is of considerable importance[45,65]. Similar phenomena are not known from single crystal data and, hence, have to be discussed in some detail.
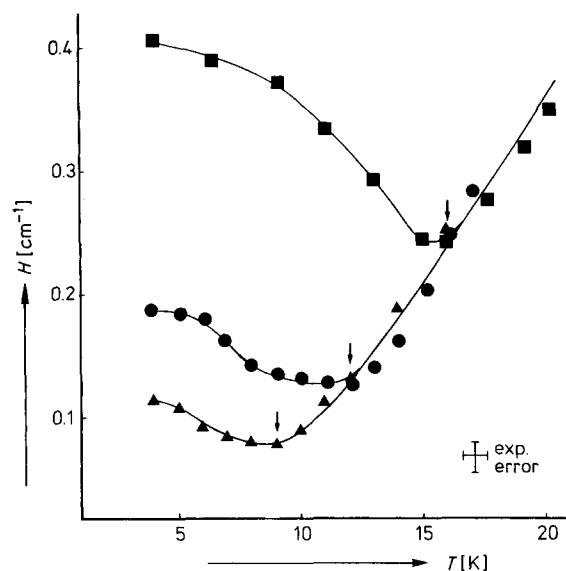
Fig. 34. Hole width as a function of temperature for phthalocyanine in polyethylene. The arrows mark the burning temperature. The increase of line width with falling temperature is rather unusual [132].

Angew. Chem. Int. Ed. Engl. 23 (1984) 113–140

133

We start with the concept that a glass can be described by a distribution of double well potentials. In this model a "particle" can tunnel from the left potential minimum to the right potential minimum: in thermal equilibrium both processes occur. Associated with the tunneling processes are changes in the optical energy of the particles, since the potential curves are different in the ground and excited states (Fig. 33a). It is evident that the tunneling dynamics do not change the total number of molecules absorbing at a given frequency and, hence, the inhomogeneous line profile does not change in time and temperature; in other words the "site population" is in a stationary state.

This situation changes if, by light irradiation, a hole is burnt into the inhomogeneous distribution. The equilibrium is then perturbed and more particles tunnel into the hole relative to those tunneling out of it. This process leads to a change in line width by spectral diffusion[124, 133, 134]. Processes of this kind are always present and can be detected with high sensitivity in hole burning experiments at low temperatures (5 K in Fig. 35a) and by subsequently cycling the temperature. At higher temperatures the rates determining spectral diffusion increase via thermally assisted processes. The glassy state moves towards a state of new quasi-equilibrium. If the temperature is recycled to the low value again, the new state is frozen in and can be evaluated spectroscopically. In the case of quinizarin, the increase in line width is a factor of two. The hole width changes irreversibly with temperature; it becomes dependent on the sample history, a characteristic feature of non-equilibrium systems.
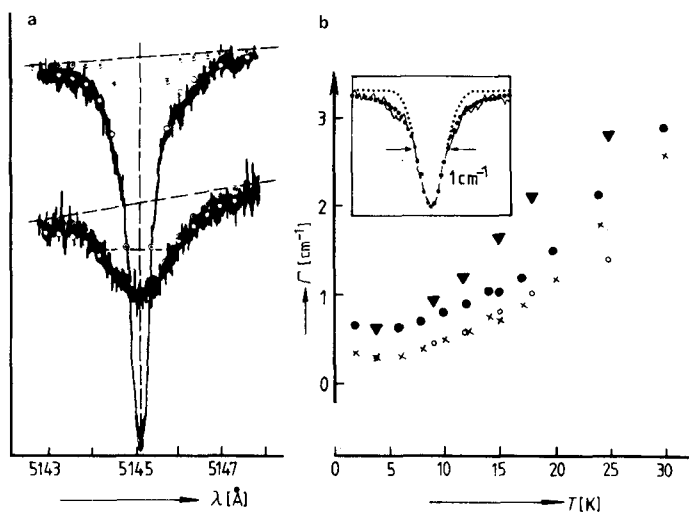
Fig. 35. a) Irreversible contributions to the line width. Both holes were burnt at ca. 5 K. The broad hole was subsequently exposed to a temperature cycle during which the sample was rapidly warmed up to 20 K. System: Quinizarin in ethanol glass [45]. b) Hole width as a function of temperature. ▲: Burning temperature equals temperature of spectroscopic experiment. ●: Burning temperature 2 K. O, × : Reduction of both curves to one master curve (good fit up to 20 K) [65]. System: Quinizarin in boric acid [45].

Because of these irreversible diffusion processes, one has to proceed with extreme care if it is desired to measure a homogeneous line width and its temperature dependence. If, for example, a hole is burned at low temperatures and one subsequently investigates the hole at higher temperatures, the result obtained differs from that had the

hole burning process been performed at each individual temperature point (Fig. 35b)[45, 65].

At present, the time scale of these diffusion processes is not known exactly. It seems that there are processes which occur on the T_1-time scale, but there are also very slow processes. The different time scales arise because of the different barrier heights and the different tunneling distances and masses.

Hole burning offers a means of investigating the time scale of such diffusion processes. It should be mentioned, however, that spectral diffusion in photochemical hole burning can be due to two different processes: It can be caused from the reorientation of molecules in the ground-state (physical dark process) and can also be caused by a back reaction from the $|P\rangle$ state to the $|R\rangle$ state (Fig. 13) (chemical dark reaction). Both processes may change the hole width in a different way.

The chemical dark reaction has been investigated in only a few systems[135, 136]. It was found for quinizarin in alcohol glasses that the reaction occurs on a logarithmic time scale (Fig. 36)[136]. Between 1.3 and 4.2 K the slopes of the logarithmic decay curves show little temperature dependence, but exhibit a pronounced isotope effect upon deuteration of the sample. We would like to discuss briefly how such a behavior can be understood.
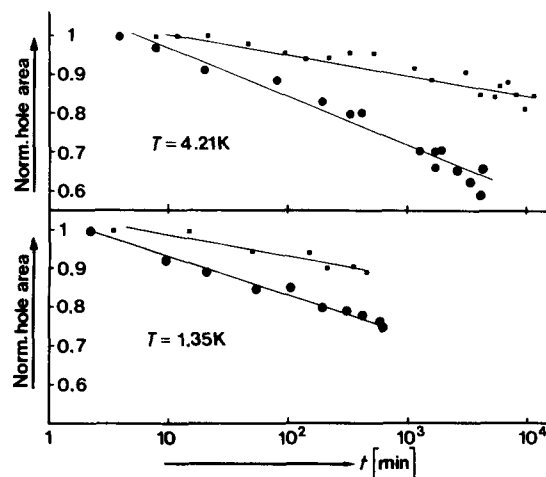
Fig. 36. Hole recovery as a function of time using the system quinizarin in ethanol-methanol glass (3 : 1) ● and in perdeuterated ethanol-methanol glass (3 : 1) ■. The slopes show a pronounced isotope effect [136].

Two main points have to be considered: a) The back reaction occurs via tunneling and b) the distribution of the reaction rates is given by the corresponding tunneling rates, as determined, for example, by measurements of the specific heat. Point a) is corroborated by the experimentally determined isotope effect. Point b) is plausible, since the back reaction, which involves reorientation of a hydrogen bond, is matrix controlled, i.e. depends on the local geometry of the solvent cage. If one accepts these assumptions, the number of molecules which have returned to the educt state after a time t can be calculated by integrating the rate distribution function:

$$\frac{n}{n_1} = N_0 \int_R^{R_1} p(R)\,\mathrm{d}R \qquad (49)$$

134

Angew. Chem. Int. Ed. Engl. 23 (1984) 113–140

where n_i is the number of molecules in the photoproduct state after a time t_1 has elapsed between hole burning and the first probing experiment. $p(R)$ is the distribution function of relaxation rates, as obtained from specific heat measurements[34–36]:

$$p(R) = \frac{\hat{P}}{2} \cdot \frac{1}{R\sqrt{1 - R/R_{max}}} \tag{50}$$

where R_{max} is the fastest relaxation rate, R_{min} is the slowest rate, and $\hat{P}$ is a constant. The constant N_0 normalizes the number of particles. It is clear that for different observation times different relaxation rates $R = 1/t$ are observed. The fastest rate which can be observed in a hole burning experiment is given by $R_1 = 1/t_1$. If it is assumed that $1/t_1$ arises because of the slow time scale of our experiment, i.e. is small compared to R_{max}, then the square root in equation (50) can be neglected. After integrating equation (49), one obtains an expression for the relative hole area which shows a logarithmic time dependence

$$\frac{A}{A_1} = 1 - \left[\ln \frac{R_1}{R_{min}}\right]^{-1} \ln \frac{t}{t_1} \tag{51}$$

From the slope of the hole decay, as given in equation (51), the ratio of the rate constants R_1/R_{min} can be estimated. The ratios vary, for the various experiments, over a vast range, i.e. 8 orders of magnitude for protonated alcohol glass and 19 orders of magnitude for deuterated alcohol glass[136]. A logarithmic decay law corresponds to the slowest possible decay kinetics. The holes therefore persist over very long time intervals.

Finally, the problem of the large optical line width of holes has to be addressed. A typical example is quinizarin, whose hole width in an EtOH/MeOH glass at 1.3 K is 0.55 cm^{-1}. Power- and saturation-broadening can be ruled out. This value is two to three orders of magnitude removed from the "Heisenberg-limit" which should be valid as $T \to 0$. The question therefore arises as to whether or not this line width can be considered as the homogeneous width. Alternatively the following situation could be conceived: It is feasible that fast spectral diffusion processes. set in immediately after the hole burning has created a non-equilibrium situation. This spectral diffusion could, in principle, also mask photochemical saturation (i.e. refilling of a hole which is close to the bottom of the band).

Spectral diffusion can also be initiated by external parameters[42, 137–140]. An ultrasonic pulse, for example, can be partly absorbed by the TLS-levels and, thus, lead to changes in the optical energy levels. Consequently, a spectral hole can be refilled by sound waves. In this respect one can look upon a hole as a "phonon memory"[42].

For a more detailed view of the optical properties of glasses it must finally be considered that not only the TLS-parameters are given by distribution functions, but also most other parameters which enter the model description (Section 9); for example, the Debye-Waller factor, the photochemical yield, and the thermal stability of the photoproduct[64]. Even the homogeneous line width need not be uniform[5]. All these parameters contribute to the spectral properties and to the time dependencies which character-

ize hole burning. It can therefore be appreciated that optical hole burning can be used as a sensitive tool for investigating subtle aspects of the physics of the amorphous state.

14. Photochemical Hole Burning in Biological Systems: Phycobiliproteins

14.1. Antenna Pigments

Chlorophyll is the most essential part of the photosynthetic reaction center, but has a comparatively low absorption coefficient in the visible spectrum. In photosynthetic organisms a great deal of the sunlight is absorbed by so-called antenna pigments. These channel the absorbed photon energy to the reaction centers. The phycobiliproteins such as phycoerythrin (PE), phycocyanin (PC), and allophycocyanin (APC) (see Fig. 37) characterize a class of antenna pigments. The pigments contain several dye molecules (chromophores) which are coupled via energy transfer processes (see e.g. [111]). The chromophores are coval-

Phycocyanobilin

Phycoerythrobilin
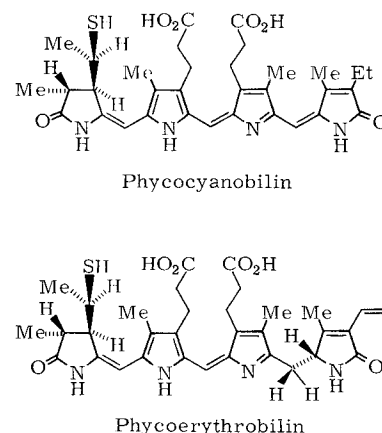
ently bound, at least at one position, to their protein environment and their excitation energy differs both due to the different micro-environment of the protein and their different structures. The energy transfer process between the chromophores is therefore non-resonant.

Conventional optical spectroscopy of antenna pigments is handicapped by low optical resolution due to the large inhomogeneous band width of the pigment spectra. Until
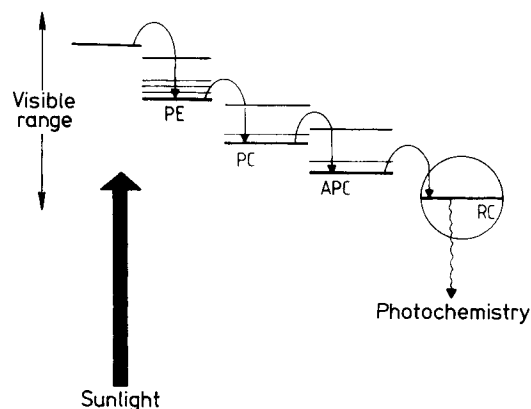
Fig. 37. Energy levels and energy transfer in the antenna pigments. PE: phycoerythrin, PC: phycocyanin, APC: allophycocyanin, RC: reaction center.

Angew. Chem. Int. Ed. Engl. 23 (1984) 113–140

135

now it was therefore impossible to investigate the spectroscopy of the various chromophores selectively. Hole burning is a new approach in this direction, because it increases the optical resolution by several orders of magnitude. The first experiments on isolated antenna pigments were published in 1981[141]. In the following section we summarize the results.

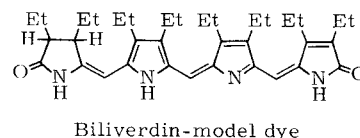## 14.2. Low Temperature Photochemistry of Antenna Pigments

Figure 38 shows a sequence of photochemical holes which have been burnt into the visible bands of phycocyanin (6270 Å) and allophycocyanin (6250 Å). The numbers label the sequence of hole burning experiments. The data indicate that the creation of a low energy hole has no influence on a hole previously burned at higher frequency; however, hole burning at high frequencies seems to partly refill holes previously burned at lower frequencies. The creation of hole 3, for example, refills hole 2, but does not affect hole 1.

Biliverdin-model dye

periments using a model chromophore. Figure 39 shows an absorption spectrum of a biliverdin dye in an alcohol glass matrix. The spectrum splits into two bands at low temperatures. It is believed that the high energy band is due to the neutral dye molecule and that the low energy band is associated with the protonated species[142]. Only the protonated form, however, exhibits PHB-photochemistry. In general, photochemical hole burning is not possible in all spectral ranges. For example, for phycocyanin within the visible spectral range of absorption, the low energy band shows efficient hole burning, whereas the high energy band exhibits no measurable photochemical yield. Possibly the corresponding chromophore is deprotonated similarly to the model dye.
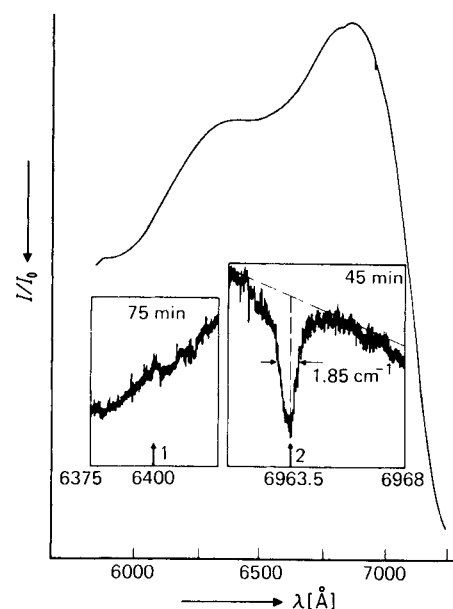

Fig. 39. Hole burning experiments using a biliverdin model dye. Only the protonated species shows measurable photochemistry (see arrow) [141]. Matrix: Ethanol-methanol glass (3 : 1), $T = 1.8$ K, resolution 0.15 Å.

Fig. 38. Photochemical holes in the lowest energy band of phycocyanin + allophycocyanin. The numbers label the sequence of hole burning events [141]. $T = 1.8$ K, resolution 0.15 Å.

From this it can be concluded that the hole burning process is photo-reversible and that the photoproduct absorbs at energies higher than the absorption energies of the educt. It appears that the photoproduct state cannot be reached directly from the excited educt state (S_1). Most probably it is reached through an intramolecular relaxation process, i.e. intersystem crossing (ISC) to the triplet state T_0. In the latter case the inverse fluorescence lifetime would be an upper bound for the photochemical reaction rate.

We believe that the case considered here is a light-induced proton transfer. This assumption is supported by ex-

14.3. Energy Transfer and Satellite Holes

Phycoerythrin behaves similarly to phycocyanin, the main difference being that hole burning occurs in both the high and low energy bands (Fig. 40). It is interesting to note that the creation of one hole at high energies leads to a whole series of holes which are displaced by ca. 600 cm^{-1} to lower energies. At first, one could attribute this phenomenon to vibronic hole burning, as described in Section 12. There are, however, several arguments which can be raised against such an interpretation, the principal one being that no vibrational transitions can be observed in the fluorescence spectrum. It is therefore more likely that the satellite holes are due to energy transfer between the various chromophores of the protein. In this case, one can distinguish three limiting cases.
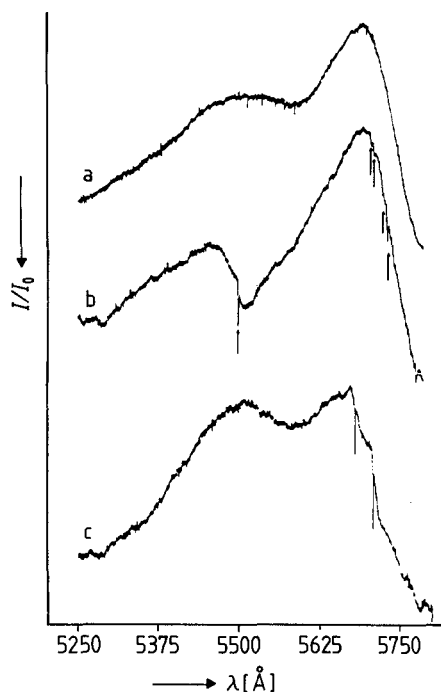
Fig. 40. Hole burning experiments using phycoerythrin [141]. a) Spectrum prior to irradiation. b) Spectrum after irradiation at 5500 Å (1 mW/cm², 10 min). The spectrum shows off-resonant satellite holes (arrows). c) Photochemical hole burning in the low energy band. No satellites appear at higher energies. Matrix: Glycerol/buffer (3 : 1), $T = 1.8$ K, resolution 0.2 Å.

a) The "fast transfer limit", which is characterized by

$$k_{ET} \gg k_{PR}$$

where k_{ET} is the energy transfer rate and k_{PR} is the rate of the photoreaction. In the "fast transfer limit" the excitation energy is transferred to the energy acceptor before a photoreaction can occur. In this case, only the satellite holes would be observed.

b) The "slow transfer limit", which is characterized by

$$k_{ET} \ll k_{PR}$$

In this case only a resonant hole can be observed.

c) The "intermediate transfer limit", which is characterized by

$$k_{ET} \approx k_{PR}.$$

In the latter case a fraction of the molecules can undergo a photoreaction in the time required for energy transfer to the acceptor molecules. Therefore resonant, as well as off-resonant, holes can be observed.

The PHB experiments in phycoerythrin can, in principle, be explained using the "intermediate transfer limit". As we discussed previously, the fluorescence rate and the photoreaction rate at 2 K must be two competing processes; this assumption is corroborated by fluorescence measurements[143]. Within the framework of the above model it is of special relevance that the satellite holes are rather nar-

row. This implies a very good correlation between the energy levels of both donor and acceptor molecules $(1 - \rho \approx 10^{-4})$. As a consequence, the local molecular environment of the chromophores must be similar, i.e. well correlated from one protein molecule to the other. This would support the concept of a highly structured protein unit with the dye molecules being surrounded by a reproducible local environment (aperiodic crystal). This unit would, to a large extent, shield the inhomogeneities of the solvent cage, at least for some of the chromophores. From these arguments one would also conclude that the energy transfer to the lowest energy chromophore is a relaxation process, which channels the energy downhill along a well defined "energy ladder". The results of polarization experiments seem to support such a view[143].

Based on the sharp structure of the zero-phonon holes, one might conclude that the fluorescence is also structured if observed under FLN conditions. This, however, has not been found for phycoerythrin and phycocyanin[144]. Obviously, there is no high degree of correlation between the absorbing and the fluorescening chromophores, which have, as a rule, the lowest energies. One might speculate that these chromophores lie close to the protein surface and are, therefore, exposed to the inhomogeneous environment of the glass matrix (glycerol/buffer solution).

15. Technical Applications

Photochemical hole burning has potentially interesting applications. Quite evident is the application for creating ultra-narrow optical filters with band widths in the MHz range. Holes could also be used as frequency markers (cf. Section 11) and for stabilizing lasers. It has been reported that holes can be used to modulate optical pulses[145, 146]. A rather attractive application has been pursued since 1978: The use of PHB for ultra-high density storage of data in the optical range[147-149]. Figure 41a shows a possible storage scheme. It consists of a spatial matrix of optical bits which can be scanned by a laser beam. If the laser hits a transmitting spot, it detects a logical 1 (an opaque spot would be 0). The highest storage density of such a scheme would be given by the minimal spot size of the laser focus,
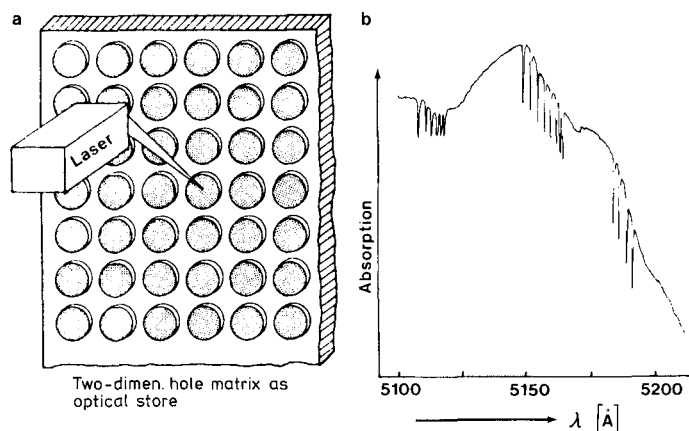

Fig. 41. a) Scheme of an optical store based on photochemical hole burning. b) Photochemical holes as bits (units of information) in the frequency domain. System: Quinizarin in ethanol-methanol glass (3 : 1, $T = 1.8$ K).

Angew. Chem. Int. Ed. Engl. 23 (1984) 113–140

137

which is in the order of λ^2, where λ is the laser wavelength (diffraction limit). The highest possible storage density using light with the wavelength of 500 nm would therefore be 10^8 bits/cm^2. If the material used in Figure 41a is replaced by one which allows hole burning, one can conceive a frequency selective storage scheme and the bit density can be increased by a factor of 10^3 to 10^4. This factor is roughly given by the ratio of the inhomogeneous line width of the storage material divided by twice the homogeneous line width. Figure 41b shows a sequence of holes burnt into the lowest absorption band of quinizarin in an ethanol/methanol glass. The figure shows that the bits can be stored in a frequency selective fashion.

In PHB-storage the frequency is used as an additional storage dimension, i.e. a two-dimensional spatial store would be three-dimensional. One could even conceive a four-dimensional store by using spatially three-dimensional holograms[150-152]. With such a method one would approach the storage density of the human brain.

The technical problems for hole burning storage are formidable. The least of these is the refrigeration of the storage material to 4 K, whereas the major problems arise from limitations in the speed of reading and writing the information. These speeds are not solely limited by frequency addressing and spatial addressing; they are also limited by the photochemical reaction rate of the photoreactive material. Last but not least, signal to noise considerations have to be discussed in detail[153]. In the technical approach to the problem great success has been achieved using frequency modulation techniques[154,155]. These methods show the feasibility of data rates in the MHz range. Simultaneous reading and writing in several "frequency channels" could possibly raise the data rates close to the GHz range.

The problems which still bottleneck the method stem from optimizing the photochemical system. It would be desirable to have an active material which operates in the wavelength range of semiconductor lasers (800-900 nm), which are cheap and can be easily tuned and modulated. In this wavelength range color centers in alkali halides have been used as active materials. These systems have the disadvantage of narrow inhomogeneous line widths and of a rather limited hole lifetime (several hours). As a result, the information density, as determined by the factor $\Gamma/2\gamma_h$, is considerably smaller than that of organic materials. Judging from these criteria, organic materials would, in principle, be preferable.

Another problem arises because frequent reading processes gradually bleach the material and, hence, destroy the information. A possible solution to this problem is to use more than one light quantum (two-photon photochemistry)[81,156]. This is illustrated in the energy level scheme in Figure 42: The frequency selective absorption of the first photon creates an intermediate state $|1\rangle$, most probably the lowest singlet state S_1; it is considered to be photostable. The photoreactive state $|a\rangle$ is reached by absorption of a second photon (Fig. 42a). This can also be reached with a second photon after a relaxation process to a long-lived intermediate state $|2\rangle$ (Fig. 42b).

Depending on the energies $\hbar\omega_1$ and $\hbar\omega_2$, the storage scheme can be designed such that irradiation to level $|1\rangle$
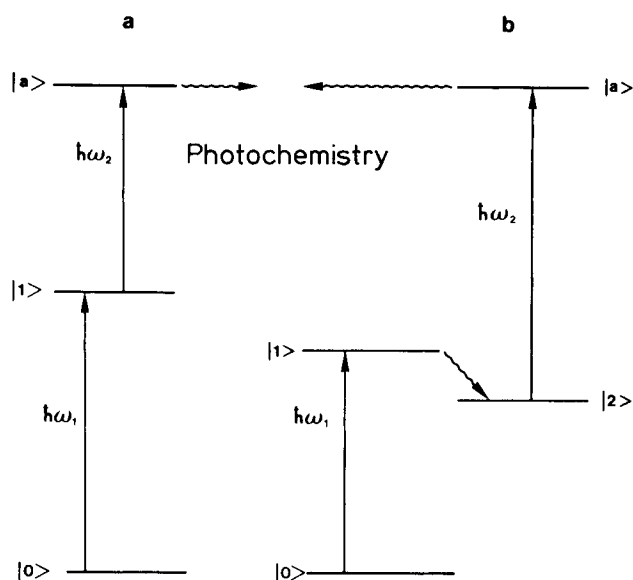

Fig. 42. Energy level scheme for hole burning via a two-photon process. a) Three-level diagram; b) four-level diagram.

does not destroy the photochemical information. The disadvantage of two-photon schemes is their low quantum yield. Similar schemes have been devised for holographic imaging techniques (two-photon, four-level scheme[156]).

From the point of view of the stability of the holes, the use of photochemical hole burning schemes appears safe. Even those photochemical holes which exhibit decay phenomena (see Section 13) decay on a logarithmic time scale, i.e. have the slowest possible relaxation mechanism.

[1] H. C. Wolf, *Adv. At. Mol. Phys. 3* (1967), 119, and literature cited therein.
[2] J. B. Birks, *J. Phys. B3* (1970) 1704, and literature cited therein.
[3] A. A. Gorokhovskii, R. K. Kaarli, L. A. Rebane, *JETP Lett. 20* (1974) 216.
[4] B. M. Kharlamov, R. I. Personov, L. A. Bykovskaya, *Opt. Commun. 12* (1974) 191.
[5] L. A. Rebane, A. A. Gorokhovskii, J. V. Kikas, *Appl. Phys. B29* (1982) 235, and literature cited therein.
[6] R. L. Garwin, *Rev. Sci. Instrum. 31* (1960) 1010.
[7] A. Götzberger, W. Greubel, *Appl. Phys. 14* (1977) 123.
[8] R. M. Schaffert, *IBM J. Res. Dev. 15* (1971) 75.
[9] W. D. Gill in J. Mort, D. M. Pai: *Photoconductivity and Related Phenomena*, Elsevier, Amsterdam 1976, p. 303.
[10] T. H. James: *The Theory of the Photographic Process*, McMillan, New York 1977.
[11] H. Scheer, *Angew. Chem. 93* (1981) 230; *Angew. Chem. Int. Ed. Engl. 20* (1981) 241.
[12] P. W. Anderson, *Phys. Rev. 109* (1958) 1492.
[13] R. Silbey in V. M. Agranovich, R. M. Hochstrasser: *Spectroscopy and Excitation Dynamics of Condensed Molecular Systems*, North Holland, Amsterdam 1983, p. 1.
[14] W. Demtröder: *Grundlagen und Techniken der Laserspektroskopie*, Springer, Berlin 1977.
[15] T. H. Keil, *Phys. Rev. A140* (1965) 601.
[16] K. Huang, A. Rhys, *Proc. R. Soc. A 208* (1951) 352.
[17] J. J. Markham, *Rev. Mod. Phys. 31* (1959) 956.
[18] D. Haarer, *J. Lumin. 18/19* (1979) 453.
[19] R. H. Silsbee in S. Nudelmann, S. S. Mitra: *Optical Properties of Solids*, Plenum Press, New York 1969, p. 607.
[20] J. B. Birks: *Photophysics of Aromatic Molecules*, Wiley-Interscience, New York 1970.

138

Angew. Chem. Int. Ed. Engl. 23 (1984) 113-140

[21] J. Jortner in B. DiBartlo: *Radiationless Processes,* Plenum Press, New York 1980, p. 103.

[22] A. S. Davydov: *Theory of Molecular Excitons,* McGraw-Hill, New York 1962.

[23] A. Abragam: *The Principles of Nuclear Magnetism,* Clarendon Press, Oxford 1961.

[24] A. Carrington, A. D. McLachlan: *Introduction to Magnetic Resonance,* Harper & Row, New York 1969.

[25] D. E. McCumber, M. D. Sturge, *J. Appl. Phys. 34* (1963) 1682.

[26] K. E. Jones, A. H. Zewail, D. J. Diestler in A. H. Zewail: *Advances in Laser Chemistry,* Springer, Berlin 1978.

[27] J. J. Sakurai: *Advanced Quantum Mechanics,* Addison Wesley, Reading 1965.

[28] R. Kubo in D. Haar: *Fluctuations, Relaxation and Resonance in Magnetic Systems,* Plenum Press, New York 1962.

[29] W. G. Rothschild, *J. Chem. Phys. 65* (1976) 455.

[30] J. Jäckle, *Phys. Unserer Zeit 12* (1981) 82, 151.

[31] G. Rehage, *J. Macromol. Sci.-Phys. B 18* (1980) 423.

[32] G. Crest, M. Cohen, *Adv. Chem. Phys. 48* (1981) 455.

[33] J. Jäckle, *Philos. Mag. B 44* (1981) 533.

[34] P. W. Anderson, B. J. Halperin, C. M. Varma, *Philos. Mag. 25* (1972) 1.

[35] W. A. Philips, *J. Low Temp. Phys. 7* (1972) 351.

[36] J. Jäckle, *Z. Phys. 257* (1972) 212.

[37] W. A. Philips: *Amorphous Solids,* Springer, Berlin 1981.

[38] S. Hunklinger, *Festkörperprobleme 17* (1977) 1.

[39] M. T. Loponen, R. C. Dynes, V. Narayanamurti, J. P. Garno, *Phys. Rev. Lett. 45* (1980) 457.

[40] M. Meissner, K. Spitzmann, *Phys. Rev. Lett. 46* (1981) 265.

[41] S. Hunklinger, M. von Schickfus in [37], p. 81.

[42] U. Bogner, *Phys. Rev. Lett. 37* (1976) 909.

[43] J. M. Hayes, G. J. Small, *Chem. Phys. 27* (1978) 151.

[44] S. K. Lyo, R. Orbach, *Phys. Rev. B 22* (1980) 4223.

[45] J. Friedrich, H. Wolfrum, D. Haarer, *J. Chem. Phys. 77* (1982) 2309.

[46] G. J. Small in [13], p. 515.

[47] R. P. Feynman, F. L. Vernon, R. W. Hellwarth, *J. Appl. Phys. 28* (1957) 49.

[48] N. A. Kurnit, I. D. Abella, S. R. Hartmann, *Phys. Rev. Lett. 13* (1964) 567.

[49] R. L. Shoemaker in J. I. Steinfeld: *Laser and Coherence Spectroscopy,* Plenum Press, New York 1978, p. 197.

[50] C. B. Harris, W. G. Breiland: *Coherent Spectroscopy in Electronically Excited States,* Plenum Press, New York 1978.

[51] G. E. Pake, T. L. Estle: *The Physical Principles of Electron Paramagnetic Resonance,* 2nd edit., W. A. Benjamin, Reading, MA 1973.

[52] R. G. Brewer, R. L. Shoemaker, *Phys. Rev. Lett. 27* (1971) 631.

[53] R. G. Brewer, R. L. Shoemaker, *Phys. Rev. A 6* (1972) 2001.

[54] J. C. McGurk, R. T. Hofmann, W. A. Flygare, *J. Chem. Phys. 60* (1974) 2922.

[55] R. G. DeVoe, A. Szabo, S. C. Rand, R. G. Brewer, *Phys. Rev. Lett. 42* (1979) 1560.

[56] A. Z. Genack, R. M. Macfarlane, R. G. Brewer, *Phys. Rev. Lett. 37* (1976) 1078.

[57] E. L. Hahn, *Phys. Rev. 80* (1950) 580.

[58] R. G. Brewer in R. Balian, S. Haroche, S. Lieberman: *Frontiers in Laser Spectroscopy, Vol. 1,* North Holland, Amsterdam 1977, p. 342.

[59] S. Voelker, R. M. Macfarlane, J. H. van der Waals, *Chem. Phys. Lett. 53* (1978) 8.

[60] R. M. Macfarlane, R. M. Shelby, *Phys. Rev. Lett. 42* (1979) 788.

[61] F. Graf, H.-K. Hong, A. Nazzal, D. Haarer, *Chem. Phys. Lett. 59* (1978) 217.

[62] R. M. Macfarlane, R. M. Shelby, *Opt. Commun. 45* (1983) 46.

[63] R. I. Personov, E. I. Al'shits, L. A. Bykovskaya, *Opt. Commun. 6* (1972) 169.

[64] J. Friedrich, J. D. Swalen, D. Haarer, *J. Chem. Phys. 73* (1980) 705.

[65] J. Friedrich, D. Haarer, R. Silbey, *Chem. Phys. Lett. 95* (1983) 119.

[66] A. Szabo, *Phys. Rev. Lett. 25* (1970) 924.

[67] L. A. Riseberg, *Phys. Rev. A 7* (1973) 671.

[68] R. I. Personov in [13], p. 55.

[69] E. I. Al'shits, R. I. Personov, B. M. Kharlamov, *Opt. Spectrosc. (USSR) 41* (1977) 474.

[70] N. Bloembergen, E. M. Purcell, R. V. Pound, *Phys. Rev. 71* (1948) 679.

[71] P. H. Lee, M. L. Skolnick, *Appl. Phys. Lett. 10* (1967) 303.

[72] A. Szabo, *Phys. Rev. B 11* (1975) 4512.

[73] H. de Vries, D. A. Wiersma, *Phys. Rev. Lett. 36* (1976) 91.

[74] S. Voelker, R. M. Macfarlane, A. Z. Genack, H. P. Trommsdorff, J. H. van der Waals, *J. Chem. Phys. 67* (1977) 1759.

[75] R. M. Hochstrasser, D. S. King, *J. Am. Chem. Soc. 97* (1975) 4760.

[76] R. Jankoviak, H. Bässler, *Chem. Phys. Lett. 95* (1983) 124, 310.

[77] M. Dubs, H. H. Günthard, *Chem. Phys. Lett. 64* (1979) 105.

[78] A. H. Weller, *Prog. React. Kinet. 1* (1961) 187.

[79] H. Beens, K. H. Grellmann, M. Gurr, A. H. Weller, *Discuss. Faraday Soc. 39* (1965) 183.

[80] D. M. Burland, F. Carmona, J. Pacansky, *Chem. Phys. Lett. 56* (1978) 221.

[81] D. M. Burland, D. Haarer: *IBM J. Res. Dev. 23* (1979) 535.

[82] G. Herzberg: *Electronic Spectra of Polyatomic Molecules,* Van Nostrand, New York 1966.

[83] J. Friedrich, D. Haarer, *Chem. Phys. Lett. 74* (1980) 503.

[84] J. Friedrich, D. Haarer, *J. Chem. Phys. 76* (1982) 61.

[85] L. Kador, Diplomarbeit, Universität Bayreuth 1984.

[86] W. Köhler, Diplomarbeit, Universität Bayreuth 1984.

[87] H. de Vries, D. A. Wiersma, *J. Chem. Phys. 72* (1980) 1851.

[88] A. U. Jalmukhambetov, I. S. Osad'ko, *Chem. Phys. 77* (1983) 247.

[89] S. Voelker, R. M. Macfarlane, *Chem. Phys. Lett. 61* (1975) 421.

[90] A. I. M. Dicker, S. Voelker, *Chem. Phys. Lett. 87* (1982) 481.

[91] A. I. M. Dicker, Thesis, University of Leiden 1982.

[92] A. A. Gorokhovskii, L. A. Rebane, *Opt. Commun. 20* (1977) 144.

[93] C. B. Harris, R. M. Shelby, P. A. Cornelius, *Phys. Rev. Lett. 38* (1977) 1415.

[94] H. M. McConnell, *J. Chem. Phys. 28* (1958) 430.

[95] A. I. M. Dicker, J. Dobkowski, S. Voelker, *Chem. Phys. Lett. 84* (1981) 23.

[96] G. W. Canters, J. H. van der Waals in D. Dolphin: *The Porphyrins, Vol. 3,* Academic Press, New York 1978, p. 531, and literature cited therein.

[97] A. I. M. Dicker, M. Noort, S. Voelker, J. H. van der Waals, *Chem. Phys. Lett. 73* (1980) 59.

[98] A. I. M. Dicker, M. Noort, H. P. H. Thijssen, S. Voelker, J. H. van der Waals, *Chem. Phys. Lett. 78* (1981) 212.

[99] A. I. M. Dicker, J. Dobkowski, M. Noort, J. H. van der Waals, *Chem. Phys. Lett. 88* (1982) 135.

[100] D. P. Burum, R. M. Shelby, R. M. Macfarlane, *Phys. Rev. B 25* (1982) 3009.

[101] R. M. Shelby, R. M. Macfarlane, *Phys. Rev. Lett. 47* (1981) 1172.

[102] A. I. M. Dicker, L. W. Johnson, M. Noort, J. H. van der Waals, *Chem. Phys. Lett. 94* (1983) 14.

[103] R. M. Macfarlane, R. M. Shelby, *Phys. Rev. Lett. 42* (1979) 788.

[104] M. D. Levenson, R. M. Macfarlane, R. M. Shelby, *Phys. Rev. B 22* (1980) 4915.

[105] R. T. Harley, R. M. Macfarlane: *High Resolution Stark Spectroscopy of the 6070 Å Color Center in NaF Using Spectral Hole Burning,* IBM Research Report, R. J. 3581, San Jose, CA 1982.

[106] R. J. A. P. Marchetti, M. Scozzafava, R. H. Young, *Chem. Phys. Lett. 51* (1977) 424.

[107] U. Bogner, R. Seel, F. Graf, paper presented at the XIIth IQEC (Int. Quantum Electronics Conf.), München 1982.

[108] U. Bogner, P. Schätz, R. Seel, M. Maier, *Chem. Phys. Lett. 102* (1983) 267.

[109] B. M. Kharlamov, L. A. Bykovskaya, R. I. Personov, *Chem. Phys. Lett. 50* (1977) 407.

[110] J. Friedrich, D. Haarer, *J. Chem. Phys. 79* (1983) 1612.

[111] St. L. Meyer, *Data Analysis for Scientists and Engineers,* Wiley, New York 1975.

[112] A. A. Gorokhovskii, J. Kikas, *Opt. Commun. 21* (1977) 272.

[113] L. A. Bykovskaya, R. I. Personov, Y. Romanovskii, *J. Appl. Spectrosc. USSR 31* (1979) 910.

[114] P. M. Selzer, D. L. Huber, D. S. Hamilton, W. M. Yen, M. J. Weber, *Phys. Rev. Lett. 36* (1976) 813.

[115] J. Szeftel, H. Alloul, *Phys. Rev. Lett. 34* (1975) 657.

[116] S. R. Kurtz, H. J. Stapelton, *Phys. Rev. B,* in press.

[117] G. E. Jellison, G. Petersen, P. C. Taylor, *Phys. Rev. Lett. 42* (1979) 1413.

[118] J. Hegarty, W. M. Yen, *Phys. Rev. Lett. 43* (1979) 1126.

[119] J. M. Hayes, R. P. Stout, G. J. Small, *J. Chem. Phys. 74* (1981) 4266.

[120] H. P. H. Thijssen, A. I. M. Dicker, S. Voelker, *Chem. Phys. Lett. 92* (1982) 7.

[121] H. P. H. Thijssen, S. Voelker, M. Schmidt, H. Port, *Chem. Phys. Lett. 94* (1983) 537.

[122] H. P. Thijssen, R. van Berg, S. Voelker, *Chem. Phys. Lett. 97* (1983) 295.

[123] F. A. Burkhalter, G. W. Suter, U. P. Wild, V. D. Samoilenko, N. V. Rasumova, R. I. Personov, *Chem. Phys. Lett. 94* (1983) 483.

[124] T. L. Reinecke, *Solid State Commun. 32* (1979) 1103.

[125] S. K. Lyo, *Phys. Rev. Lett. 48* (1982) 688.

[126] P. Reineker, H. Morawitz, *Chem. Phys. Lett. 86* (1982) 359.

[127] H. Morawitz, P. Reineker, *Solid State Commun. 42* (1982) 609.

[128] I. Osad'ko, S. A. Zhadnov, *Opt. Commun. 42* (1982) 185.

[129] B. Jackson, R. Silbey, *Chem. Phys. Lett. 99* (1983) 381.

[130] S. Alexander, R. Orbach, *J. Phys. Paris Lett. 43* (1982) L-625.

[131] S. K. Lyo, R. Orbach, unpublished.

[132] A. R. Gutierrez, G. Castro, G. Schulte, D. Haarer in P. Reineker, H. Haken, H. C. Wolf: *Electronic Excitations and Interaction Processes in Organic Molecular Aggregates,* Springer, Berlin 1983.

[133] J. L. Black, B. I. Halperin, *Phys. Rev. B 16* (1977) 2879.

[134] S. Hunklinger, M. Schmidt, *Z. Phys. B,* in press.

Angew. Chem. Int. Ed. Engl. 23 (1984) 113–140

139

[135] E. Cuellar, G. Castro, *Chem. Phys. 54* (1981) 217.

[136] W. Breinl, J. Friedrich, D. Haarer, unpublished.

[137] U. Bogner, R. Schwarz, *Phys. Rev. B24* (1981) 2846.

[138] U. Bogner, G. Röska, *Thin Solids Films 99* (1983) 257.

[139] U. Bogner, G. Röska, *J. Lumin.*, in press.

[140] H. Lengfellner, T. R. Gosnell, R. W. Tkach, A. J. Sievers, *Appl. Phys. Lett. 43* (1983) 437.

[141] J. Friedrich, H. Scheer, B. Zickendraht-Wendelstadt, D. Haarer, *J. Am. Chem. Soc. 103* (1981) 1030; *J. Chem. Phys. 74* (1981) 2260; *J. Lumin. 24/25* (1981) 815.

[142] H. Scheer, W. Kufer, *Z. Naturforsch. C 32* (1977) 513.

[143] B. Zickendraht-Wendelstadt, J. Friedrich, W. Rüdiger, *Photochem. Photobiol. 31* (1980) 367.

[144] C. Kerling, Diplomarbeit, Universität Bayreuth 1983.

[145] A. Rebane, R. Kaarli, *Chem. Phys. Lett. 101* (1983) 317.

[146] A. Rebane, R. Kaarli, P. Saari, A. Anijalg, K. Timpmann, *Opt. Commun. 47* (1983) 173.

[147] G. Castro, D. Haarer, R. M. Macfarlane, H. P. Trommsdorf, US-Pat. 4101976 (1978).

[148] D. Haarer, *SPIE J. 177* (1979) 97.

[149] A. R. Gutierrez, J. Friedrich, D. Haarer, H. Wolfrum, *IBM J. Res. Dev. 26* (1982) 198.

[150] R. J. Collier, C. B. Burckhardt, J. H. Lin: *Optical Holography*, Academic Press, New York 1971.

[151] W. J. Tomlinson, E. A. Chandross, *Adv. Photochem. 12* (1980) 201.

[152] H. J. Schmitt, *Phys. Unserer Zeit 12* (1981) 3.

[153] G. C. Bjorklund, G. Castro: *Frequency Domain Optical Storage*, IBM Research Report R.J. 3287 (39813), San Jose, CA 1981.

[154] G. C. Bjorklund, W. Lenth, C. Ortiz, *SPIE J. 298* (1981) 107.

[155] W. Lenth, C. Ortiz, G. C. Bjorklund, *Opt. Commun. 41* (1982) 369.

[156] G. C. Bjorklund, C. Bräuchle, D. M. Burland, D. C. Alvarez, *Opt. Lett. 6* (1981) 159; C. Bräuchle, D. M. Burland, *Angew. Chem. 95* (1983) 612; *Angew. Chem. Int. Ed. Engl. 22* (1983) 582.
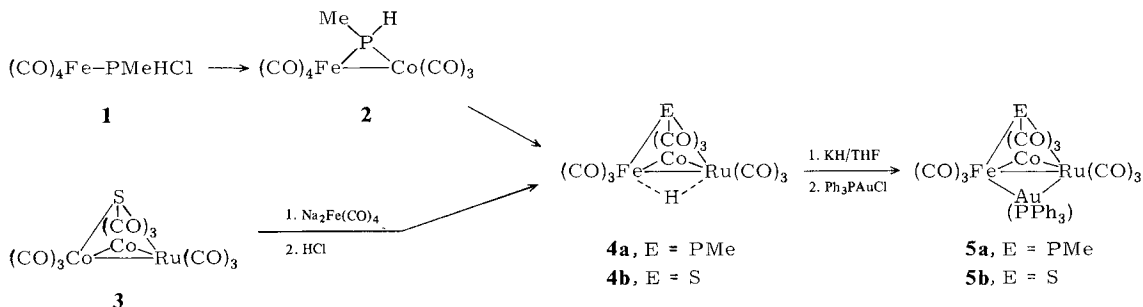
COMMUNICATIONS

Stepwise Assembly of a Cluster with Four Different Metal Atoms**

By *Klaus Fischer, Manfred Müller*, and *Heinrich Vahrenkamp*[*]

Heteronuclear organometallic clusters lend themselves more readily to systematic synthesis[1] and to mechanistic reactivity studies[2] than homonuclear compounds. Their chemistry still presents many challenges, and we have now met one of these: the stepwise synthesis of a cluster having four different metal atoms from four simple precursors.

The cluster 5a is formed from the synthetic building blocks $MePCl_2$, $Fe_2(CO)_9$, $KCo(CO)_4$, $Ru_3(CO)_{12}$, and Ph_3PAuCl. We have previously described the reaction sequence reproduced in simplified form in Scheme 1 as far as compound 4a[3]. Deprotonation of 4a with KH and subsequent treatment with Ph_3PAuCl led to black 5a[4]. An alternative route to the cluster type 5, involving a metal exchange reaction[2,5], has been found for the μ_3-sulfido complex 5b: 4b is formed from 3 (cf. Scheme 1) and can be converted into black-red 5b (yield 37%) by analogy to 4a[6].

The constitutions of 5a and 5b were confirmed by X-ray structure analysis. A simplified molecular structure of 5a is shown in Figure 1. Because of disorder, in the completely analogous structure of 5b only the heavy atom framework could be determined unequivocally[7]. Like the

Scheme 1. Synthetic pathway to the clusters 5.

[*] Prof. Dr. H. Vahrenkamp, Dipl.-Chem. K. Fischer, Dr. M. Müller
Institut für Anorganische und Analytische Chemie der Universität
Albertstrasse 21, D-7800 Freiburg (FRG)

hydride ligand in 4a, the Ph_3PAu moiety preferentially adopts an edge-bridging site, and hence the heteronuclear tetranuclear clusters 5 exhibit a "butterfly" arrangement of the metal atoms.